Remote sensing of potential biosignatures from rocky, liquid, or icy (exo)planetary surfaces

Olivier Poch[1]*, Joachim Frey[2], Isabel Roditi[3], Antoine Pommerol[4], Bernhard Jost[4], and Nicolas Thomas[4]

[1] Center for Space and Habitability, Universität Bern, Sidlerstrasse, 5, 3012 Bern, Switzerland

[2] Institute of Veterinary Bacteriology, University of Bern, Länggassstrasse 122, 3012 Bern, Switzerland

[3] Institut für Zellbiologie (IZB), Baltzerstrasse 4, 3012 Bern, Switzerland

[4] Physikalisches Institut, Universität Bern, Sidlerstrasse, 5, 3012 Bern, Switzerland

*Corresponding author:

Olivier Poch, NCCR PlanetS, Physikalisches Institut, Universität Bern, Sidlerstrasse, 5, 3012 Bern, Switzerland, Phone: +41 31 631 33 93; Fax: +41 31 631 33 93; Email: olivier.poch@csh.unibe.ch

Running title: *Remote sensing of surface biosignatures*

Abstract:

To detect signs of life by remote sensing on objects of our solar system and on exoplanets, the characterization of light scattered by surface life material could complement possible clues given by the atmospheric composition. We reviewed the reflectance spectra of a broad selection of major biomolecules that constitute terrestrial carbon-based life from 0.4 to 2.4 μm, and we discuss their detectability through atmospheric spectral windows. Biomolecule features in the near-infrared (0.8-2.4 μm) will likely be obscured by water spectral features and some atmospheric gases. The visible range (0.4-0.8 μm), including the strong spectral features of pigments, is the most favorable. We investigated the detectability of a pigmented microorganism (*Deinococcus radiodurans*) when mixed with silica sand, liquid water, and water ice particles representative of diverse surfaces of potentially habitable worlds. We measured the visible to near infrared reflectance spectra (0.4-2.4 μm) and the visible phase curves (at 0.45 and 0.75 μm) of the mixtures to assess how the surface medium and the viewing geometry affect the detectability of the microorganisms. The results show that ice appears to be the most favorable medium for the detection of pigments. Water ice is bright and featureless from 0.4 to 0.8 μm, allowing the absorption of any pigment present in the ice to be well noticeable. We found that the visible phase curve of water ice is the most strongly affected by the presence of pigments, with variations of the spectral slope by more than a factor of 3 with phase angles. Finally, we show that the sublimation of the ice results in the concentration of the biologic material onto the surface and the consequent increase of its signal. These results have applications to the search for life on icy worlds, such as Europa or Enceladus.

Keywords:

Remote Sensing; Biosignatures; Reflectance Spectroscopy; Exoplanets; Spectroscopic Biosignatures; Pigments

1. Introduction

The search for a second origin of life on another world is a major goal of space exploration. Life as we know it requires liquid water, organic compounds (carbon-based molecules), and sources of energy to emerge. The presence of liquid water is an indispensable condition for the formation and the activity of the macromolecules that constitute terrestrial-like living systems (proteins, RNA, DNA and their ancestors) (Bartik et al., 2011). Such conditions could be found on rocky planets that can sustain liquid water on their surfaces, such as Earth, and also on icy moons or rocky planets that can sustain liquid water only in their interiors (Cockell et al., 2016).

For example, in our solar system, Mars is a rocky planet located at the rim of the habitable zone that might have sustained Earth-like habitable conditions at its surface in the past and might still be habitable today in its subsurface (Westall et al., 2013). Additionally, some icy satellites of Jupiter and Saturn, in particular Europa and Enceladus, possess internal salty water reservoirs in contact with silicates (Zolotov and Kargel, 2009; Hsu et al., 2015), opening the possibility of chemical exchanges and energy sources favorable to the emergence and the sustainability of life (Hand et al., 2009), although this is still under debate (Pascal, 2016). Habitable worlds of such nature, as well as Earth-like worlds that are able to maintain their habitability for billions of years, may also be found around other stars.

To infer the presence of potential habitats and life on these objects, remote sensing at visible and near infrared wavelengths (Vis-NIR) is often the first source of information available. In our solar system, remote sensing observations of planetary surfaces are often thought to be precursors of *in situ* analyses that guide the selection of landing sites. In the case of exoplanets, the search for signs of life can only rely on remote sensing techniques.

What is the potential of these techniques to infer the presence of life? Vis-NIR remote sensing observations could reveal the presence of certain gases in the atmosphere and/or of specific surface features potentially produced by forms of life.

In the near term, the search for biosignatures in exoplanets will first focus on the retrieval of the atmospheric composition through transmission observations. H_2O, CO_2, or CH_4 are major greenhouse gases that can contribute to long term stability of surface liquid water, an important parameter for habitability (Kaltenegger and Selsis, 2007). Moreover, gases such as O_2/O_3 and CH_4 could be produced by life. But confirming their biogenic origin will require ruling out their possible production via abiotic processes such as geology or atmospheric chemistry (Tian et al., 2014; Wordsworth and Pierrehumbert, 2014; Domagal-Goldman et al., 2014; Harman et al., 2015). For example, Domagal-Goldman et al. (2014), Tian et al. (2014) and Harman et al. (2015) suggest that detection of a sufficient mixing ratio of CH_4 may rule out a scenario of abiotic production of O_2. Other, more specific biogenic gases, such as dimethyl sulphide, methanethiol, or methyl chloride, could also be searched for, but they require special environmental conditions to build up to more detectable amounts than are possible on Earth (Segura et al., 2005; Domagal-Goldman et al., 2011; Seager, 2014).

With the development of direct-imaging observations, possible clues obtained by the detection of life-related gases in the atmosphere would be satisfactorily complemented by reflectance spectra of the surface. Indeed, if the composition of the atmosphere is such that the surface can be probed, and if life is present and abundant on it, the light scattered by the surface may contain spectral signatures of those biomolecules that constitute living organisms (Dalton et al., 2003). The observation of such signatures could provide a direct indication of the presence of life on a planetary surface. Moreover, as explained by Cockell (2014), some inhabited worlds may have biogenic gases that are indistinguishable from abiotic gases or at

undetectable concentrations, in which case probing the surface would be desirable. On Earth, the "red-edge" produced at 0.7 μm by vegetation (due to chlorophyll absorption and to the structure of leaves) (Seager 2005; Kiang et al., 2007) is widespread at the surface and is detectable from space (Sagan et al., 1993) and in the disk integrated spectrum of the planet (Arnold et al., 2002; Woolf et al., 2002; Montañés-Rodríguez et al., 2006; Tinetti et al., 2006; Arnold, 2008; Sterzik et al., 2012). However, structured land ecosystems, including photosynthetic plants, colonized Earth's continents only 470 My ago (Labandeira, 2005). For most of the 4.5 Gy of Earth's history, life was unicellular, mainly present in liquid bodies, and possibly in ice during "Snowball Earth" events when the surface was globally covered by a thick ice shell (Campbell et al., 2011; Pierrehumbert et al., 2011; Cayol et al., 2015). In these ancient times, Earth may have exhibited different surface spectral signatures of life, in particular spectral features in the Vis-NIR due to pigment biomolecules of photosynthetic (Kiang et al., 2007) or non-photosynthetic (Schwieterman et al., 2015) organisms. These spectral features are characterized by strong absorbance in shorter wavelengths and a more or less pronounced rise in reflectance toward the red or NIR, which we will term generally here as "red slopes." Sanromá et al. (2013; 2014) and Schwieterman et al. (2015) modeled the photometry and the disk-averaged spectra of such early-Earths or potential Earth-like exoplanets, including full radiative transfer and analysis of the effect of rotation and/or phase. They show that the color due to the presence of pigmented microorganisms may be detectable in some conditions, especially if the microorganisms are widespread and abundant enough on the surface. From a technological point of view, obtaining Vis-NIR spectral data of the surface of an exoplanet with enough precision to identify such signatures will be extremely challenging (Fujii et al., 2010; Kawahara and Fujii, 2010; Fujii and Kawahara, 2012; Cowan and Strait, 2013), but may be achievable in the future by using, for example, a large UV/optical/near-infrared space telescope (see the "LUVOIR Surveyor" projects, e.g.,

Dalcanton et al., 2015). As the number of discovered exoplanets continues to increase and the observation techniques become more and more accurate, rocky planets of Earth-masses are being detected (Howard et al., 2013; Pepe et al., 2013) including some in the "habitable zone" (Quintana et al., 2014). Moreover, astronomical observations have recently reached a level of precision that allows the collection of the tiny reflected star light from an exoplanet (Evans et al., 2013; Martins et al., 2015; Shporer and Hu, 2015).

Surface biosignatures would be easier to detect on objects of our own solar system with the use of probes that can orbit or fly-by planets or moons. However, exploration of the solar system has shown that only Earth currently exhibits a widespread surface biosignature (the vegetation "red-edge"). *If signs of life are present on other solar system objects, they are only at local spots on surfaces of particular types*. For example, on icy worlds such as Europa and Enceladus, the local upwelling or eruption of subsurface material (Dalton et al., 2003; Porco et al., 2006; Dalton et al., 2010; Roth et al., 2014) suggests that, if present in the subsurface, traces of life (in the form of chemical wastes or remains of whole organisms) may be locally exposed at the surface.

Thus, considering the history of life on Earth (first present in the ocean, then on rocky surfaces and maybe on ice) and other potentially habitable places in the solar system (rocky Mars, icy moons), surface biosignatures may be present and potentially detectable on at least three types of surfaces: rocky, liquid water, and water ice. Extrasolar systems may be populated by similar or other types of habitable planets or moons that exhibit these three types of surfaces. For example, global water ocean planets could exist, although their potential to host life is unknown (Léger et al., 2004; Lammer et al., 2009). Large oceans could also exist on cold tidally locked planets in the habitable zone of M dwarfs. On these cold "eyeball planets," water could form a global ice shell with a liquid ocean at the sub-stellar point

(Pierrehumbert, 2011), and life could exist in the ocean and in the ice shore (Angerhausen et al., 2013). Moreover, several studies highlight that the first characterization of a habitable planet is more likely to take place around an M dwarf because of the higher abundance of M stars and greater ease of observation, but not because M star planets are more hospitable to life, which they may not be (Scalo et al., 2007; Tarter et al., 2007; Segura et al., 2010; Kopparapu, 2013).

What signal can be expected from the observation of signs of life embedded in rocky, liquid water, and water ice surfaces via Vis-NIR remote sensing techniques?

Prior works on surface biosignatures have focused largely on spectral properties of pure samples of micro-organisms. Dalton et al. (2003) measured the reflectance spectra of pure biomolecules and three colonies of micro-organisms frozen at 120 K. Hegde et al. (2015) measured the spectra of 137 living micro-organisms at room temperature. But these samples were pure micro-organisms, measured independently of their environmental background. Cockell et al. (2014) measured the spectral "red slopes" of three colonies of pigmented micro-organisms mixed in silica sand, but only from 0.4 to 0.8 μm and without considering phase angle dependence. Furthermore, to our knowledge, no study has addressed the possibility of detecting hints of life by remote sensing in the ice produced by the eruption of subsurface liquid water on active icy worlds like Enceladus or Europa. As a consequence, the present study seeks to expand the existing data on potential surface biosignatures with laboratory measurements at a wider wavelength range (from 0.4 to 2.4 μm), considering phase angle dependency, and taking into account the environmental context of these signatures, namely, the compositions of the atmosphere and of the surface medium. To answer the question above, we examined the relative detectability of a pigmented microorganism on rocky, liquid water, and water ice surfaces.

First, we review the spectral features we can expect from the major biomolecules that constitute terrestrial life, and we discuss their detectability (through spectral windows) depending on the atmospheric composition of the host planet. We argue that biomolecules having extended conjugated systems, also called pigments, represent one of the most accessible signatures by remote sensing. Then, we focused our work on a single microbe, *Deinococcus radiodurans*, taken as a general model of pigmented micro-organisms. The reflectance of all pigmented microorganisms is characterized by a spectral "red slope" in the visible, although shifted in wavelength and with a different shape depending on the micro-organism (Hegde et al., 2015). Moreover, all micro-organisms possess quite similar near-infrared spectra because they are made of the same types of organic molecules (Dalton et al., 2003). *Deinococcus radiodurans* is popular in the field of astrobiology because it is a poly-extremophile bacterium that shows remarkable resistance to ionizing radiation, desiccation, and UV radiation (Makarova et al., 2001). It has been used in many previous studies (Dalton et al., 2003; Cockell, 2014; Schwieterman et al., 2015), so our results can be compared with others. We performed laboratory measurements to investigate the detectability of *Deinococcus radiodurans*, as a model of pigmented microorganisms, in various surface types that may be encountered in the habitable planetary environments described above, namely, silica sand (rocky continental-like surface), liquid water, and water ice particles. The Vis-NIR reflectance spectra and the variability of the pigment spectral slope depending on phase angle are assessed. The results show that ice appears to be the most favorable medium in which to detect pigmented micro-organisms. First, the visible spectral red slope of pigmented micro-organisms could be more easily detected in water ice particles than in silica sand. Second, the visible phase curve of ice is significantly influenced by the presence of the pigments. Third, ice can undergo the sublimation process, resulting in the concentration of biologic material on the surface and the consecutive increase of its signal. Additionally, we show that silica sand

and semi-conductor minerals in general are unfavorable to the detection of the visible red slope, but could be more favorable to the detection of near-infrared absorption bands of biomolecules, provided that the micro-organisms are in desiccated forms. Finally, we discuss the potential of glint on liquid water surfaces to provide indications of the presence of suspended pigmented microorganisms.

The results of these laboratory measurements may be of interest for the upcoming exploration of icy worlds of the solar system, such as Europa and Enceladus, and space missions planned in the near-future. In the longer term, these results could also guide exoplanetary observations. Taken together, the review of the reflectance of the main carbon-based biomolecules, combined with our review of gas absorption ranges (section 1), the measurements of the Vis-NIR reflectance and phase curves of a pigmented micro-organism in various surface media (section 2), and the discussion on the feasibility of discriminating false positives (section 3), would provide observers with indications as to what signal to expect and on how to progress towards remote detection of life.

2. Materials and Methods

2.1. Sample preparation

Biomolecules. To obtain reflectance spectra of pure biomolecules, identify their specific spectral features and gain insights into the spectra of whole micro-organisms, dry powders of some examples of the most abundant categories of molecules of terrestrial life were purchased from Sigma-Aldrich and Bachem (see chemical structures and references in Supplementary Table S1):

- Proteins, polymers of amino acids (polypeptides), are the most abundant constituents of living organisms (~50% of the dry mass of a cell, Alberts et al., 2013). We chose bovine serum albumin, representative of simple polypeptides, and human haemoglobin, representative of polypeptides associated with cofactor molecules that have an extended conjugated system. Haemoglobin is a polypeptide associated with protoporphyrin IX molecules linked to Fe^{2+}, also called haems.
- Deoxyribonucleic acid (DNA). DNA and ribonucleic acid (RNA) comprise ~23% of the dry mass of a cell. We measured deoxyribonucleic acid sodium salt from calf thymus.
- Lipids are the main constituents of cell membranes (~7% of the dry mass of a cell). We chose two phospholipids representative of those used by all domains of terrestrial micro-organisms: 1,2-dipalmitoyl-rac-glycero-3-phosphatidic acid disodium salt, which is a phospholipid with an ester bond, used by Eukaryota and Bacteria, 1,2-dihexadecyl-rac-glycero-3-phosphocholine, which is a phospholipid with an ether bond, used by Archaea.
- Carbohydrates are the most abundant biomolecules on Earth because of their huge production by plants (otherwise they represent ~7% of the dry mass of a cell). We chose to measure cellulose.
- Biomolecules that have an extended conjugated system, pigments (<1% of the dry mass of a cell, but with a strong spectral feature at Vis-NIR wavelengths). We chose two porphyrins, a class of molecules universal in terrestrial biology as part of proteins involved in energy production: protoporphyrin IX with Fe^{3+} (haemin) and chlorophyllin sodium copper salt. We also chose retinal, representative of another class of pigments called carotenoids.

Each powder was deposited as an optically thick layer in the field of view of the SCITEAS imaging system described below to measure their Vis-NIR reflectance spectrum.

***Deinococcus radiodurans* mixed with liquid water.** *Deinococcus radiodurans* strain n°ATCC-1393 was obtained from LGC Standards, Teddington, Middlesex TW11 0LY, UK, and grown in Columbia broth (DIFCO 294420, Becton Dickinson, Spraks, MD, USA) supplemented with 1% glucose at 30°C with gentle rotation to end the exponential growth phase. After growth, the bacteria were washed in deionized water by repeated centrifugation and re-suspension to obtain final suspensions of *D. radiodurans* suspensions at 10^{10} and 10^{11} org./mL. Only the suspension at 10^{10} org./mL was used for the measurements presented in this paper. Typical concentrations of microorganisms range from 10^4 to 10^5 /mL in oceans (Ting et al., 2002) and up to 10^8 /mL in lakes (Cayol et al., 2015). We chose very high concentrations (also for *D. radiodurans* mixed in silica sand and ice) because our goal was first to perform a sensitivity testing of the presence of 10^{10} org./g *D. radiodurans* in different surface media to discern which media are more or less favorable to their detection via remote sensing. The bacterial density (org./mL) was determined with a Petroff-Hausser bacterial counter chamber (A.H. Thomas Company, Philadelphia, PA, USA). In parallel, the concentration of colony forming units (cfu/mL) was determined on Columbia broth-agar medium showing that 70% of the organisms determined were viable. Reflectance measurements were carried out on the flat surface (2×6 cm) of a volume of suspension that filled a container 2 cm deep. The walls of the container were coated with a spectrally featureless dark surface. The same container filled with the same volume of deionized water served as a reference.

Pure *Deinococcus radiodurans* hydrated/desiccated. Samples of pure *D. radiodurans* were produced in two different ways: the first resulted in a hydrated deposit, the second in a

desiccated deposit. The hydrated deposit was produced by centrifugation of a suspension in a tube whose internal surface was coated with a plastic film holding a spectrally featureless dark surface. During centrifugation, an optically thick deposit of bacteria formed on the dark surface. After centrifugation, the liquid supernatant was discarded, then the deposit was removed from the tube and its reflectance spectrum was measured. The desiccated deposit was obtained by sedimentation and evaporation of a 1 mL water suspension containing 10^9 org./mL inside a 1 cm diameter cylindrical plastic container. After complete desiccation of the *D. radiodurans* layer, this non-optically thick dry crust was placed on a spectrally featureless dark surface prior to the measurement.

***Deinococcus radiodurans* mixed with silica sand.** *D. radiodurans* was mixed with silica sand (150-630 μm, 329 μm on average (Babu et al., 2014), Sigma-Aldrich, n°274739) via a liquid suspension that was homogenized and evaporated at 50°C to obtain sand particles coated with dry bacteria at 10^{10} org./g ≈ 10^{10} org./mL (the silica sand density is 1.5 g/mL). This concentration is the upper limit for microorganisms in natural terrestrial soils, which usually ranges from 10^8 to 10^{10} /mL (Torsvik et al., 1990). A sample of sand that was free of *D. radiodurans* was prepared by using the same procedure but with pure deionized water, to serve as a reference.

***Deinococcus radiodurans* in water ice grains.** The samples of *D. radiodurans* embedded in water ice were obtained by nebulizing into liquid nitrogen suspensions of bacteria in deionized water at 10^6, 10^8, and 10^{10} org./mL. This preparation technique, which has been used in previous studies (Poch et al., 2016a; b), was chosen to be representative of how icy particles could be formed from the eruption of subsurface liquid water (potentially containing bacteria or pigments) on active icy worlds like Enceladus or Europa. The liquid suspensions were maintained under magnetic stirring for homogenization in a spray bottle that was

connected via a tube to an ultrasonication device and placed inside a freezer. The liquid was pumped into a sonotrode where it was spread out as a thin film on the nozzle surface and disintegrated into micro-droplets by the ultrasonic vibrations. Those droplets fell directly into a stainless steel vessel filled with liquid nitrogen and froze instantly. Microscopy images of the ice particles produced by this method indicate a mean diameter of 67µm with a standard deviation of 31µm (see Fig. 1b in Poch et al., 2016a). The particles are perfectly spherical with smooth surfaces. Pure water ice particles were also produced by using the same method, to serve as a reference. Once produced, the ice particles were stored for some minutes in liquid nitrogen before being deposited in their sample holders for the reflectance measurements. The bulk density of the ice particles samples was 0.5 g/mL, giving concentrations of *D. radiodurans* of about 10^5, 10^7, and 10^9 org./mL in each ice sample. Typical values of concentrations for microorganisms in or on terrestrial surface ices range from 10^2 to 10^5 /mL (Cayol et al., 2015). The very high concentration of 10^9 org./mL was chosen to compare the results with the similar concentrations (~10^{10} org./g) used in the other surface media. Following the results of this sensitivity test, which show that water ice is the most favorable media to detect remotely the visible spectral slope of *D. radiodurans*, we then produced a water ice sample at a more realistic concentration, down to 10^5 org./mL.

----Figure 1 should be here----

2.2 Reflectance measurements

Reflectance spectra (0.4-2.4 µm) of the biomolecules powders and *D. radiodurans* samples were measured with the SCITEAS imaging system shown in **Erreur ! Source du renvoi introuvable.**a and described by Pommerol et al. (2015). It consists of a tunable monochromatic light source (the light of a 100 W Quartz Tungsten Halogen lamp is dispersed and filtered by a monochromator producing the desired monochromatic light from 0.4 to 2.4

μm, and focused on a fibre bundle) that illuminates the entire surface of the sample, and two cameras: one covering the visible spectral range (0.38–1.08 μm) and the other the near-infrared spectral range (0.85-2.4 μm). The cameras were positioned above the sample at an angle of about 13° from the nadir direction. The hyperspectral cubes were acquired with a spectral sampling resolution of 20 nm from 0.38 to 0.96 μm and 10 nm from 0.96 to 2.4 μm. White Spectralon™ plates (Labsphere) were used as external and internal calibration standards. In the reduced dataset, absolute uncertainty on the calibrated reflectance factor is ±0.1, and the spatial variability of the reflectance across the field of view is of the order of 10%. Thus, the SCITEAS imaging system does not provide an accurate measurement of the absolute reflectance, but it provides a spectrum resolved in wavelength from 0.4 to 2.4 μm. Accurate measurements of the reflectance factor were obtained with the PHIRE-2 radio-goniometer (see section 2.4).

2.3 Sublimation experiment

The three samples of water ice particles containing *D. radiodurans* at different concentrations, plus the pure water ice sample, were deposited in a sample holder composed of four compartments. The preparation of the samples took place in a freezer, at about -100°C. The sample holder containing the four samples was then rapidly transferred inside the SCITEAS thermal vacuum chamber where they were allowed to sublime under a pressure of 10^{-6} mbar and a temperature below -70°C. The evolution of the reflectance of the samples during sublimation was monitored *in situ* by the cameras, through a large quartz window (see **Erreur ! Source du renvoi introuvable.**a). More details on the systems of the simulation chamber and the data acquisition can be found in the work of Pommerol et al. (2015).

2.4 Phase curves

The PHIRE-2 radio-goniometer, shown in **Erreur ! Source du renvoi introuvable.**b and described by Pommerol et al. (2011) and Jost et al. (2016), was used to measure the absolute reflectance of the samples by using a 250W tungsten-halogen lamp with two bandpass filters (maximum of transmission centered at 0.45 and 0.75 µm, with FWHM of 0.07 µm) at two different fixed incidence directions (0 and 60°), and by scanning emission angles from -80° to +80°. The angular sampling in emission was of 5°, and was reduced at 0.5° around opposition (or 1° for liquids, in order to reduce the measurement time and avoid sedimentation of the suspension). The data calibrated in units of the radiance factor (RADF) were systematically converted to the "reflectance factor" (REFF), as defined by Hapke (1993). The reflectance factor is measured with relative errors of 1 to 2%. The whole instrument is installed in a freezer, which allowed us to perform measurements on the water ice samples containing *D. radiodurans* at -35°C at atmospheric pressure.

The two bandpass filters were chosen in order to measure the reflectance shortward and longward of the spectral slope due to pigments of *D. radiodurans* occurring from 0.5 to 0.65 µm. From the reflectance values measured at 0.45 and 0.75 µm, we computed the relative spectral slope, or "relative magnitude of slope", S_r (in %/100 nm):

$$S_r = \frac{R_{0.75} - R_{0.45}}{R_{0.45} \times (750 - 450)} \times 10^4 \qquad \text{(Equation 1)}$$

For additional information, we also define and show the data of the "absolute spectral slope" in the Supplementary Material document, section S3.

3. Reflectance of biomolecules and atmospheric spectral windows in the Vis-NIR

This part 3 provides detailed background for the experiments performed on the pigmented bacteria *D. radiodurans* mixed with surface media, whose results are presented in section 4. In this section, we review the existing knowledge on Vis-NIR remote sensing of biomolecules, whole organisms, and atmospheric spectral windows. We describe the results obtained by previous studies and complement them by some new measurements and discussions.

----Figure 2 should be here----

----Table 1 should be here----

3.1. Reflectance of biomolecules

All terrestrial living organisms consist mainly of liquid water and ~14% specific carbon-based biomolecules susceptible to giving spectral features in the Vis-NIR. Proteins, DNA, and RNA comprise around 73% of the dry mass of an average cell (Alberts et al., 2013). The membrane constituents, mainly lipids and carbohydrates, represent around 14%, and the remaining 13% are composed of ions and small carbon molecules, including molecules that have an extended conjugated system, also called pigments. Reflectance spectra of the main components of cells were measured by Dalton *et al.* (2003) (a phospholipid, DNA, protein and carbohydrate). Here, we measured these spectra to have our own data set collection, and we expanded it by including additional biomolecules (another phospholipid, a pigmented-protein, and several pigments) and by considering the issue of atmospheric gases on their remote detectability.

Fig. 2a shows the reflectance spectra of some examples of the main biomolecules, which were measured at room temperature with the SCITEAS imaging system. All of the biomolecules have absorption bands in the near infrared due to combination tones and overtones of mainly C–H, O–H, and N–H stretching modes (Workman Jr and Weyer, 2012). The constituents of the cell membrane, phospholipids, are characterized by relatively narrow C–H absorption bands at about 1.2, 1.4, 1.7, 1.9, and 2.3 μm. Those C–H absorptions are also observed for all the other biomolecules. The difference of chemical structure (ether bond instead of an ester bond) between the phospholipids of Archaea and those of Eukaryota and Bacteria does not produce a significant difference in their Vis-NIR reflectance spectra. DNA exhibits only two major absorptions centered at 1.47 and 1.92 μm, possibly due to N–H and POH stretching, respectively, and/or to water of hydration. All proteins are characterized by two absorptions of low intensity at 2.05 and 2.17 μm, due to the specific peptide bond that links the amino acid monomers, constituting their polymeric structure. Carbohydrates, such as cellulose, exhibit the C–H absorptions and are characterized by a strong absorption centered at 2.1 μm, due to O–H combination. Finally, biomolecules that have extended conjugated systems (pigments), like porphyrins (chlorophyllin, hemin) and carotenoids (retinal), give strong absorptions in the visible range due to electronic transitions in their molecular orbitals. The absorbance in the visible is due to Gaussian-shaped absorbance by pigment absorbance bands, with several pigment bands clustering in the visible, which results in broad absorbance. The tendency toward higher reflectance toward the red and NIR is due to the declining absorbance of pigments and to increased scattering (Kiang et al., 2007). In vivo, this scattering is controlled by the properties of cell walls and the structure of the assembly of cells (i.e., colony of bacteria or plant's leaf). Given their ability to absorb visible light, pigments play a central role in light-harvesting organisms (phototrophs) by converting light into metabolic energy. But beyond photosynthesis, porphyrins are universal in terrestrial

biology, as part of proteins involved in energy production processes, from methanogenesis to respiration (Milgrom, 1997). The spectral position of the red slope due to porphyrins changes depending on its ligands (transition metal at the center of the macrocycle, protein environment) as seen in Fig. 2a for protoporphyrin IX as hemin or in haemoglobin. The position of the red spectral slope of pigments will change depending on their chemical environment: if they are within a cell (in vivo) or if they are present just as molecules outside the cell (in vitro). This shift can be of the order of 0.1 μm (see for example Fig. 3 of Chen and Blankenship, 2011). Because of their ubiquitous distribution in life on Earth, biomolecules similar, though not necessarily identical, to existing bio-porphyrins may have evolved on other planets as well, if life ever arose there. Besides porphyrins, other pigments are found in terrestrial life and have many functions such as acquisition of energy by phototrophic organisms; acquisition of nutrients; and protection against ultraviolet radiation, oxidants, extremes of heat and cold, and other microbes (Liu and Nizet, 2009).

It is worth noting that most of the functions listed above demonstrate that pigments are also useful for sub-surface chemotroph life forms. Thus, it makes sense to search for bio-pigments that might be exposed at the surface of inhabited icy worlds following an eruption or ejection event. The terrestrial biomolecules measured here are the outcome of a chemical evolutionary process that happened under the peculiar environmental conditions of early Earth. If another form of carbon-based life occurred elsewhere in liquid water, the detailed structure of its biomolecules would probably be different from the terrestrial ones. However, whatever their detailed structures, the wavelength ranges of their Vis-NIR spectral signatures will be similar because, as organic molecules, they would contain C–H, O–H, N–H bonds and conjugated systems. Table 1 summarizes the wavelength ranges of interest for probing surface biosignatures from 0.4 to 2.4 μm.

3.2. Reflectance of whole microorganisms

Dalton et al. (2003) measured the reflectance spectra of three microbial colonies frozen at 120 K. They showed that the three colonies possess quite similar near-infrared spectra, because they are made of the same types of organic molecules (Fig. 2a) as every terrestrial life forms including extremophiles. For all the micro-organisms tested, they detected absorptions of hydrates, but also absorption features at 2.05 and 2.17 μm, due to proteins, and at 2.3 μm due to C–H bonds (see Fig. 2 in Dalton et al., 2003). However, these absorptions are absent in the spectra of 137 living microorganisms measured at room temperature by Hegde et al. (2015) (see Fig. S1). These discrepancies between different studies may result from the difference of temperature, from different water contents of the bacteria colonies, or from the culture medium used to grow the microorganisms, which is exceptionally rich in peptides. To avoid a possible bias in the present work, prior to the measurements, we washed with pure water the liquid medium used to grow the *Deinococcus radiodurans* bacteria as described in section 2. The reflectance spectrum of the hydrated bacteria (Fig. 3a) is presented in **Erreur ! Source du renvoi introuvable.**a. The spectrum is dominated by the red slope occurring from 0.5 to 0.65 μm due to the absorption by the carotenoids pigments synthesized by *Deinococcus radiodurans* (deinoxanthine, phytoene, and astaxanthin among others, see Lemee et al., 1997 and Lysenko et al., 2011) and by strong water absorption bands. The collection of carotenoids contained in *D. radiodurans* appears to have absorption maxima at 0.4-0.42 μm and 0.48-0.5 μm, creating a small bump of reflectance at 0.44 μm. Because of the water, biomolecules absorption bands cannot be seen in the near infrared (a weak absorption at about 1.77 μm is due to liquid water, see Fig. S1). Thus, this reflectance spectrum is similar to those presented by Hegde et al. (2015) (see Fig. S1), and does not show the absorptions due to proteins, contrary to the findings of Dalton et al. (2003). Conversely, the reflectance spectrum obtained after desiccation of the bacteria

(Fig. 3a) reveals all the absorption bands expected from the biomolecules, including proteins (Fig. 4a). Dry residues of dead microorganisms or microorganisms in dormant mode, like spores, may have a signature close to that of this desiccated sample, which allows for more features to be visible in the infrared compared to living organisms. However, in both desiccated and hydrated cases, the spectral signatures of pigments are clearly noticeable in the visible range.

3.3. Influence of atmospheric composition on the detectability of surface biosignatures

Fig. 2b shows the spectral ranges where the absorption cross sections of several gases potentially found in the atmosphere of a habitable planet if higher than 10^{-24} cm^2/molecule and peak to a maximum. The cross sections were obtained from the HITRAN database (Rothman et al., 2009) via the Virtual Planetary Laboratory website* and via the work of Burrows (2014). Of course, the actual spectral windows will depend on the concentration of the gases, which are not taken into account here. The goal of Fig. 2 is to propose a convenient and quick way to identify potential spectral windows through which remote surface biosignatures could be searched for. Spectral windows are not completely transparent, however, and wavelengths immediately adjacent to spectral windows are not completely opaque. A more detailed characterization of the spectral windows would require modeling of the radiative transfer through the atmosphere as presented for example in the works of Montañés-Rodríguez et al. (2006), Sanromá et al. (2014), and Schwieterman et al. (2015).

We expect to find water vapor in the atmospheres of exoplanets that we hope to characterize for biosignatures as our searches will emphasize water-bearing planets. After taking into account the ranges where water vapor absorption is maximal, only two spectral windows remain in the near infrared with which to look for biosignatures (1.5-1.8 μm and

* http://depts.washington.edu/naivpl/content/molecular-database

2.0-2.3 μm), while most of the visible range is still accessible (from 0.4 to 1.1 μm). The spectral window in the visible range allows us to look for the presence of pigments; the one at 1.5-1.8 μm provides access to a C–H absorption band and the one at 2.0-2.3 μm provides access to the absorption bands of proteins and carbohydrates (see Fig. 2b).

The presence of additional gases (CO_2, CO, CH_4, etc.) will further reduce these spectral windows, especially in the infrared. In an atmosphere that has an Earth-like composition (H_2O, CO_2, and O_2), only spectral windows at about 1.65-1.8 μm and 2.1-2.3 μm enable inquiry for potential surface biosignatures in the near-infrared. For example, from Earth orbit, the satellite Hyperion is able to probe the surface reflected light in these spectral windows with a spectral resolution high enough to study the cellulose and protein contents of the vegetation (Liebig et al., 2012). For a planet with an atmosphere of more reduced composition, the detection of the surface could be more challenging. Fig. 2 shows that the simultaneous presence of H_2O, CH_4, and H_2 in an atmosphere could completely mask any surface biosignature in the near infrared. Moreover, atmospheres that have reduced or neutral compositions are susceptible to produce organic aerosols due to the irradiation by UV photons or charged particles (Cleaves et al., 2008). Such aerosols can scatter the light and significantly reduce the reflected radiance in the whole UV-Vis-NIR range, preventing the detection of the surface as clouds also do.

Fig. 2b shows that the surface reflected light is significantly more accessible in the visible than in the near infrared range. Consequently, the best chance to find a surface biosignature is to look for the reflectance of pigments in the visible range. The surface reflected light in the visible could be affected by the presence of ozone (O_3) and nitrogen dioxide (NO_2), also by Rayleigh scattering of the atmosphere. Rayleigh scattering produces an increase of reflectivity in the near-UV and is characterized by a blue slope from 300 to 550

nm in the case of Earth (Crow et al., 2011). The occurrence of both atmospheric Rayleigh scattering and surface pigments results in a break of slope in the visible part of the reflectance spectrum, as seen for example in Fig. 5 and 7 in the work of Schwieterman *et al.* (2015). Given enough spectral resolution, this break of slope could be indicative of the presence of surface pigments.

For atmosphere-less planets, like icy habitable worlds, the entire Vis-NIR spectral range is accessible. However, the wavelength range available for characterization of the surface also depends on the light provided by the host star and, here, the visible wavelength range seems preferable. Indeed, Sun-like stars emit most of their light at visible wavelengths. By contrast, cool stars (i.e., M dwarf stars) emit in the NIR, and the habitable zones of these stars are at such small separations they will not be amenable to observations by the next generation of space-based coronagraph instruments (see Robinson et al., 2016).

4. Results: Reflectance of *Deinococcus radiodurans* in silica sand, liquid water, and water ice

4.1. Reflectance spectra from 0.4 to 2.4 μm

Fig. 4 (b, c, d) shows the reflectance spectra of mixtures of *Deinococcus radiodurans* with silica sand, liquid water, and water ice. Reflectance spectra of pure *D. radiodurans* (Fig. 4a) and pure media are also shown as references. Note that Fig. 4 shows normalized reflectance. For comparison of the absolute levels of reflectance between samples, the reader should use the reflectance factors measured by the PHIRE-2 radio-goniometer at a given phase angle (Fig. 7, 8, and 9). The concentration of bacteria used in the mixtures is extremely

high compared to most natural environments on Earth (see section 2.1). Our goal in the present study was to assess what potential surface biosignature might be observed in each medium in best case scenarios. The influence of the concentration will be discussed later in section 5.

----Figure 3 should be here----

----Figure 4 should be here----

4.1.1. Bacteria mixed with silica sand grains

The reflectance spectrum of pure silica sand (Fig. 4b) exhibits a red slope from 0.4 to 1.3 µm (due to charge transfer absorptions) and absorption bands of traces of phyllosilicates centred at 1.41 µm (O-H stretching), 1.92 µm (combination of structural O-H and adsorbed H-O-H stretching modes), and 2.20 µm (metal-OH band) (Clark, 1999). When mixed with 10^{10} *D. radiodurans*/mL, the red slope of bacteria can be distinguished at 0.55 µm, superimposed on the slope of the sand. From 1.9 to 2.4 µm, the absorptions of the proteins, carbohydrates, and lipids of *D. radiodurans* are superimposed on the phyllosilicates absorption bands. It should be noted that in the mixture of sand and *D. radiodurans* presented in Fig. 4b, the *D. radiodurans* are present in dry form (section 2.1). As discussed above, in the case of hydrated *D. radiodurans* mixed with sand, the absorption bands from 1.9 to 2.4 µm would be masked by the water of hydration.

4.1.2. Bacteria mixed with liquid water

In the presence of 10^{10} org./mL *D. radiodurans*, the red slope of the pigment is noticeable from 0.4 to 0.6 µm. The fact that it is less steep than for the other samples is due to

a longer growth phase of *D. radiodurans* before reaching stationary phase in this experiment, resulting in lower carotenoids concentrations.

4.1.3. Bacteria mixed in water ice particles

Pure water ice particles (Fig. 4d) show strong absorption bands at 1.03, 1.26, 1.50, and 2 μm, but are bright and featureless from 0.4 to 0.8 μm. As a consequence, the reflectance spectrum of water ice particles that contain inclusions of *D. radiodurans* at 10^9 org./mL clearly shows the pigment absorption at 0.55 μm. However, no absorption of any biomolecule was detected in the near infrared part of the spectrum. In particular, we searched for the narrow absorption features at 2.05 and 2.17 μm due to the amide bonds of the proteins that constitute *D. radiodurans*, which were described by Dalton et al. (2003) in the spectrum of a frozen colony of *D. radiodurans* at 120 K, but these features are absent of our spectra. This is due to the fact that our sample is made mainly of water ice, which masks the NIR absorption bands of *D. radiodurans* included in it, while the Dalton *et al.* sample was a concentrated colony that was not mixed with additional water.

These reflectance spectra indicate that the "red slope" due to the pigment of *D. radiodurans* is potentially detectable in all of these media, given a high concentration of bacteria. At lower concentrations, which are more probable, this red slope is much more difficult to extract from the signal. For example, 6a shows that water ice grains containing 10^7 org./mL only exhibit a weak red slope. One option for addressing this problem would be to determine if, and how, the magnitude of this "red slope" changes depending on the viewing geometry. Is there a viewing geometry for which the red slope is maximized? In addition, water ice is a medium that can be affected by sublimation, and this process could also enhance the concentration and consequently the signal of the biosignatures at the surface.

4.1.4 Influence of sublimation on the detectability of pigments embedded in ice.

Sublimation, the phase transition from solid to gas, occurs extensively on ice deposits present on bodies that have no or low atmospheric pressure, such as Mars (Byrne, 2009; Byrne et al., 2009) or on the surface of icy satellites of the solar system (Moore et al., 2009). On icy satellites, any ice ejected from the subsurface, potentially including biomolecules, will eventually sublime at the surface. Sublimation also occurs on current Earth in localities with very low humidity and/or very low temperatures, such as the dry valleys in Antarctica, arid regions of continental interiors, and mountaintops (Marchant et al., 2002; Reba et al., 2012). Sublimation is also relevant during Snowball Earth events (Campbell et al., 2011). Thus, the range of environmental conditions in which sublimation occurs is relatively broad.

To test the influence of the sublimation process on the detectability of pigmented bacteria present inside the ice, we prepared samples of water ice particles containing 10^9, 10^7, and 10^5 bacteria per milliliter (see section 2), after which the samples were allowed to sublime during 13 hours inside the SCITEAS simulation chamber under about 10^{-6} mbar and -70°C.

----Figure 5 should be here---

----Figure 6 should be here---

Fig. 5 shows the samples before and after sublimation. As the water sublimes, the non-volatile components, here the *D. radiodurans* bacteria, initially embedded in the ice are deposited at the surface, forming a so-called sublimation lag deposit. The reflectance spectra presented in Fig. 6a show that this process significantly increases the detectability of the spectral red slope due to the pigment even if they are initially present at low titers in the ice. After the sublimation of the top ~5 mm of ice, Fig. 6b shows that the value of the spectral

slope from 0.40 to 0.62 μm has increased by a factor of ~2 for the samples at 10^9 and 10^7 org./mL. For the sample at 10^9 org./mL, an increase of 50% is observed.

In previous studies (Poch et al., 2016a, 2016b), we showed that the sublimation of ice particles that contain abiotic organic pigments (tholins) and minerals also leads to the formation of porous sublimation residues that have a stronger visible spectral red slope but very low, or even totally absent, absorption bands in the near infrared. We attributed these very faint absorption bands in the near infrared to the sub-micrometric size of some of the non-volatile particles combined with the porous nature of the sublimation residues (Poch et al., 2016b). Although *D. radiodurans* bacteria are expected to be larger than 1 μm, they also form porous residues after sublimation (see Fig. 5), and we did not detect any near infrared absorption band due to biomolecules in the reflectance spectra of these sublimation residues after sublimation of the top ~5 mm of the ice.

4.2. Influence of the viewing geometry on the pigment's spectral slope.

We analyzed the light scattered by the samples of sand, liquid water, and water ice mixed with *D. radiodurans* for two different incidence angles (0° and 60°) and at two wavelengths (0.45 and 0.75 μm), before and after the slope. The phase curves measured at 0° and 60°, and the resulting relative spectral slope profiles are presented for all media in Fig. 7, Fig. 8, and Fig. 9. The phase angle is defined in Fig. 1a. These data have been deposited on the Data Analysis Center for Exoplanets (DACE) (https://dace.unige.ch/lossy/index) where they can be freely visualized and downloaded.

4.2.1. Bacteria mixed with silica sand grains

The phase curve of pure sand is characterized by an opposition peak at low phase angles and by a forward scattering behavior (Fig. 7a). Pure sand has an intrinsic spectral slope of maximum 17 %/100 nm whose profile over emission angles is arc-shaped at 0° and 60° incidence (Fig. 7b). At 60° incidence, the spectral slope is maximal at ~60° phase angle. At the zero phase angles, the spectral slope of pure sand has a local minimum. The spike in slope over 0-5° phase angle is due to the higher amplitude of the opposition peak at 450 nm than at 750 nm. When 10^{10}org./mL *D. radiodurans* are present, the phase curves show similar arc-shaped profiles and opposition peaks. The spectral slope is increased by about +10 %/100 nm between 0 and 60°. However, this increase is less pronounced for higher phase angles: only +5 %/100 nm at 135° phase angle for 60° incidence.

Fig. 7 shows that, except for the increase of spectra slope, the presence of 10^{10} org./mL *D. radiodurans* has no significant impact on the shape of the phase curve of the silica sand. This shape, like an arch, is due to the phase reddening effect, attributed to semi-transparent, smooth, and spectrally red particles, as detailed in the work of Schröder et al. (2014). This effect is not fully understood.

----Figure 7 should be here----

4.2.2. Bacteria mixed with liquid water

The light scattering properties of *Deinococcus radiodurans* suspended in liquid water are presented in Fig. 8. We also measured pure water as a reference. For pure water, the variations of the reflectance and slope with phase angle are due to the scattering of the light on the borders of the container filled with the water. The suspension of *D. radiodurans* is much more turbid, so its data only appear to be affected by the borders of the container at 450

nm from 65 to 80° phase angle. The spectral slope of the suspension is constant over the whole range of phase angles, with a value comprised between 13 and 26 %/100 nm.

The main characteristic of the phase curves shown in Fig. 8 is the presence of a "mirror-like reflection" of the incident light beam by the surface of the suspension, also called "specular reflection" or "glint." At the specular point, the reflectance reaches very high values. However, the signal acquired by the PHIRE-2 radio-goniometer, which has not been designed to measure specular reflectance, is affected by instrumental artifacts that prevent us from drawing any definitive conclusion on the spectral slope at this peculiar geometry.

----Figure 8 should be here----

4.2.3. Bacteria mixed in water ice particles

The phase curve of pure water ice particles (spherical, 67±31 μm diameter) is characterized by an opposition peak at low phase angles and a strong forward scattering behavior (Fig. 9a). In the presence of 10^9 org./mL *Deinococcus radiodurans*, the reflectance of the ice is significantly reduced both at 0.45 and 0.75 μm, and the shape of the phase curves is also affected. At 0° incidence, the branches of the phase curves get more curved in the presence of bacteria compared to their rather linear shape in pure ice (see Fig. 10). At 60° incidence, the ice is more forward scattering in the presence of bacteria (see Fig. 9a, right panel). The dependence of the spectral slope of the ice with phase angle dramatically changes in the presence of bacteria. At 0° incidence, pure water ice has a slightly negative spectral slope (about -1 %/100 nm) rather constant with phase angle, which becomes strongly positive (about +11 %/100 nm) in the presence of *D. radiodurans*. More interestingly, at 60° incidence, while pure water ice has also a spectral slope of about -1 %/100 nm, which is constant with phase angle, it becomes strongly positive (up to +16 %/100 nm) and arc-shaped

with a maximum at about 60° in the presence of *D. radiodurans* (see Fig. 9b, right panel). This shape resembling an arch is due, as for the sand, to the phase reddening effect (Schröder et al., 2014). We note that the amplitude of the arch (i.e., the difference of spectral slope between 60° and 140°/0°) is of about 12 %/100 nm, as for the sand containing *D. radiodurans*, which suggests that this amplitude could be a parameter directly controlled by the pigmented microbes, even in silica sand. However, in term of relative amplitude of spectral slope (i.e., the ratio of spectral slope between 60° and 140°/0°), the arch of the sample of *D. radiodurans* in water ice is two times more contrasted (ratio of 3.4) than that of the sample in sand (ratio of 1.8). It is also interesting to note that, at 60° incidence geometry, the spectral slope is inversely correlated with the reflectance: the slope is maximum at the phase angle where the reflectance is minimum (Fig. 9b,c, right panel). Finally, it is important to note that these features are not unique to pigmented bacteria and can also be produced by abiotic pigments (such as *tholins*, i.e., complex mixture of abiotic organic molecules produced by irradiation of ices or gases).

----Figure 9 should be here----

----Figure 10 should be here----

5. Discussion: Possibilities and limitations for remote detection of microbial surface biosignatures

5.1. Phase angle dependence of the spectral slope of pigments in different surface media

The best geometry to detect the spectral slope of a pigment can be defined as the one for which both the reflectance and the spectral slope are maximal. Table 2 shows that in most

cases such ideal configuration does not exist, except for water ice at 0° incidence angle and 0° phase angle. At 60° incidence angle, for sand and ice, high phase angles (140°) provide the higher reflectance signal, but the spectral slope is maximum at around 60°, because of the phase reddening effect (Schröder et al., 2014). For liquid water, the specular direction provides the highest reflectance of all media, but the contribution of the pigment to the color of the specular beam is unknown and should be studied further. The maximum variation of relative spectral slope depending on viewing geometry is obtained for water ice at 60° incidence: the red slope is a factor of 3 higher at 60° than at 0 and 140° phase angles (see Fig. 9b, right panel). The results given in Table 2 could be used to estimate at which phase angles the red slope, due to a hypothetical pigmented microorganism present at the surface, would be maximized.

Opposition geometries, with phase angles around 0°, can be reached for objects of our solar system, but they would be extremely rare and difficult to achieve for extrasolar observations (the phase angle of a maximally inclined system (i = 90°) with the planet seen at superior conjunction would be close to 0°). The data presented in Table 2 can be mainly useful for solar system observations and in particular for observations of the icy surfaces of Europa or Enceladus.

In the field of exoplanets, these data could be of interest for the analysis of the phase curves of rocky, liquid, or icy objects. Indeed, as an exoplanet orbits its parent star (with an orbit edge-on with respect to the observer), the phase angle (defined here as the angle between the star and the observer) at which the observer sees its surface changes from low (around conjunction) to high (around opposition) phase angles. To determine the variations of the spectral red slope in the reflected light spectrum of an exoplanet covered by pigments as it orbits its host star, one should compute the disk integrated spectrum of the planet at different

phase angles, using Bidirectional Reflectance Distribution Functions (BRDF) (see for example Doughty and Wolf, 2010). The phase curves presented in Fig. 7, 8, and 9 show partial extracts of the full BRDF of surface samples containing pigmented microorganisms. Future laboratory work should determine the full BRDFs as inputs for numerical simulations of the phase curves of the disk integrated spectra of exoplanets.

5.2. Discriminating false positives.

An important issue to consider when searching for reliable remote sensing biosignatures is the possibility of false positives. Abrupt changes of the reflectance from 0.4 to 1.2 μm, produced by biogenic pigments, can also be produced by semiconductor minerals having a band gap of energy comparable to a photon at these wavelengths such as iron oxide or sulphur (Seager et al., 2005). In the case of a mixture of a semiconductor mineral and a biopigment, the spectral slope of the biopigment would be masked by the one of the mineral. A possible strategy to disentangle both spectral slopes might be to try to fit the data with reference spectra of known minerals (such as the one of Clark, 1999). However, given the high number of uncertainties such as grain size, number, and exact nature of the mineral phases, this strategy would be very challenging. False positives also exist in the near infrared range. For example, kaolinite, a type of phyllosilicate, has an absorption band centered at 2.17 μm (Clark et al., 2007), exactly as proteins do (see **Erreur ! Source du renvoi introuvable.** and Fig. 2a). Observations at other wavelengths can help to discriminate kaolinite from proteins (absence of the other band of proteins at 2.05 μm, presence of an absorption centered at 2.21 μm, absent in biomolecules). The C–H absorption bands at around 1.2, 1.4, 1.7, 1.9, and 2.3 μm are quite specific to organic matter, although it cannot be distinguished between biotic and abiotic origin. In all these cases, a study of the broader context of the object (e.g., the presence of an atmosphere and its composition) may help to assess the probability of the

signal being a biosignature versus a false positive. Another possibility could be to analyze the polarization of light reflected by potential surface biosignatures. Indeed, all the asymmetric organic molecules that constitute living systems (so-called chiral molecules) are only present in one of their two possible geometries (a property called homochirality), and this asymmetry can induce the reflected light from a living system to be partially polarized in a specific way. Several studies have shown that circular polarization is detected in the light scattered by photosynthetic microbes and is more intense near the red slope of the pigment reaching a degree of circular polarization of 0.01 to 0.1% (Sparks et al., 2009a; Sparks et al., 2009b; Martin et al., 2010; Martin et al., 2016). Interestingly, iron oxide and sulphur do not exhibit an intense signal of circularly polarized reflected light (~ 0.004 %) (Sparks et al., 2009a; Sparks et al., 2009b). Existing spectro-polarimeters used in astronomy can measure degrees of circular polarization down to 0.0001% (Hough et al., 2006), but the main problem will be to accumulate a sufficient number of photons from an exoplanet to reach this level. According to Sparks et al. (2009), very large ground based telescopes such as the upcoming 39-m European Extremely Large Telescope would have sufficient light to perform these observations only if a very favorable target exists (i.e., a planet covered with biopigments orbiting a star in the solar neighborhood whose light could be well separated from the star), which will be extremely challenging. In the near future, it is more probable that circular polarimetry could be used in our solar system for the exploration of Mars, Europa, or Enceladus. Sparks et al. (2012) presented a concept of compact and robust spectropolarimeter that could be used to probe the surface of solar system objects from orbit or *in situ*. Alternatively, the degree of linear polarization of the scattered light could also be significantly more prominent in biological (degree of linear polarization $\geq$ 50% for plant leaves and flower petals) versus mineral samples (degree of linear polarization < 50%) as shown in the work of Berdyugina et al. (2015). Although linear polarization is not specific to homochirality and would not allow a

reliable discrimination of biotic from abiotic materials, it might facilitate the detection of biopigments in the solar system and extra-solar observations conducted in the near future.

Consequently, polarization and in particular circular polarization could potentially be a way to discriminate biotic and abiotic spectral signatures. All the features discussed in the present paper (spectral red slope of pigment, absorption bands of biomolecules in the near infrared, phase curves, specular reflection over liquid water, biomolecules embedded in ice) should be analyzed for their degree of polarization to provide more guidance for the observers. In the context of the search for such a signal on Earth-like exoplanets, the question of the influence of the atmosphere (via molecular scattering, scattering by dusts) on the polarization signal should also be assessed via numerical modeling (García Muñoz, 2015) or observations of Earth's surface from space.

5.3. The issue of signal intensity and the concentration of surface life.

The detection of a surface biology would be strongly dependent on the intensity of the signature it can produce, linked to its extent and concentration at the planetary surface. Today, and probably only since 470 My ago (Labandeira, 2005), the "red-edge" produced at 0.7 μm by vegetation is detectable from space in the disk integrated spectrum of Earth (Sagan et al., 1993; Montañés-Rodríguez et al., 2006; Tinetti et al., 2006). During most of the 4.5 Gy of Earth's history, however, life was unicellular and mainly present in liquid bodies. Schwieterman et al. (2015) demonstrated that, in a best case scenario where the Earth oceans are filled with a high concentration of pigmented microorganisms, the red slope of the pigment could be detected in the disk average spectrum of Earth. However, the global extent of microbial oceanic life that populated early Earth is unknown. In addition to the global extent of surface life, the local concentration of this life in the surface medium will also

influence the intensity of the reflected signal. As indicated previously, the concentration of bacteria of 10^9-10^{10} org./mL used in the mixtures whose spectra are presented in Fig. 4 is extremely high compared to most of the natural environments on Earth where it ranges from 10^2 to 10^{10}/mL. Cockell *et al.* (2014) measured the reflectance spectrum of silica sand at a concentration of *D. radiodurans* of 10^8 /mL and indicated that the characteristic spectral feature of the pigment was indistinguishable from the sand spectrum. Indeed, the electronic absorption processes of minerals resulting in absorptions and slopes in the visible (such as crystal field effects, charge transfer, conduction bands, or color centers, see Clark et al., 1999) can make it very difficult to detect pigmented life forms on a rocky surface.

5.4. The more favorable cases of icy and possibly liquid surfaces.

In contrast to rocky surfaces, water ice offers a bright and featureless baseline in the visible that could make it easier to detect pigments embedded in it. If pigmented organisms or isolated bio-pigment molecules are present on icy surfaces (because they thrive there or, more probably, because they have been ejected from the subsurface and deposited at the surface), remote techniques could possibly detect hints of their presence. For example, on Earth, the red-pigmented alga *Chlamydomonas nivalis* is a cold-tolerant microbe that grows on snow fields and glaciers, and it can be detected and quantified from satellite observations (Takeuchi et al., 2006). In the case of icy worlds similar to Europa or Enceladus, the detection of potential bio-pigments might even be facilitated by the lack of atmosphere. We have shown that the sublimation of the ice, a process that is occurring on Europa and possibly on Enceladus, can concentrate bio-pigments at the surface and enhance their detectability even if they are initially present at concentrations of 10^7/mL or 10^5/mL in the ice. However, the global extent of these potential signatures could be quite low, and their detection might be hindered by the presence of salts, minerals, or other abiotic organics in the ice. In addition, the

processing of surface deposits by irradiation (ultraviolet photons, energetic particles) could also destroy or change the structure of biomolecules. Future work should assess the effect of these mixtures and processes on the detectability of bio-pigments in ice.

In the near infrared, we did not observe any superposition of absorption bands of the other biomolecules constitutive of *D. radiodurans* with the absorption bands of the water ice, even after sublimation of about 5 mm of ice. As a consequence, it seems that only water-poor areas at the surface of icy worlds could allow the detection of other biomolecules in the near infrared, such as amide bonds due to proteins as proposed by Dalton et al. (2003).

Finally, liquid water surfaces might be the best candidates to overcome this issue of signal intensity thanks to specular reflection, also called glint. Given that Earth is the only planet that has stable bodies of liquid water at its surface in the solar system, observation of glints over liquid water surfaces would only be relevant for exoplanetary observations. Williams and Gaidos (2008) first proposed that glints could be observed from distant exoplanets, and Robinson et al. (2014) validated glint detection using interplanetary spacecraft observations of the disk-averaged spectrum of Earth.

Although glints are considered as undesirable contaminants in remote sensing of Earth (Miller et al., 2007), could they be indicative of the composition of the water, namely, the presence of suspended pigmented micro-organisms? Specular reflected photons only interact with the very surface of the water, so they contain less information on the constituents of the water than diffusely reflected photons that penetrate deeper. However, according to the Fresnel equations (Hecht, 2002), the intensity of the specular reflection depends on both the angle of incidence and the refractive index of the reflecting surface, also known as the real part (n) of the optical index. The real part (n) is dependent on the wavelength and is linked, by

causality (cf. Kramers-Kronig relations), to the imaginary part of the optical index (k) representing the absorption of the light by the medium. In practice, n exhibits an inflection point at a wavelength where k is maximal (Hale and Querry, 1973). So a liquid water surface that contains pigments and exhibits a strong red slope due to absorption by the pigments may have an optical index (n) showing a bump centered at the wavelength of the slope. According to the Fresnel equations, this variation of optical index may induce a variation of the intensity of the specular reflectance. The possibility to retrieve compositional information by analyzing the wavelength dependence of specular reflection should be explored further, especially in polarized light, given the fact that specular reflections are highly polarized (Williams and Gaidos, 2008). Future works should also address how much signal would be observed in the visible wavelengths by a glint over an exoplanetary ocean. For example, Williams and Gaidos (2008) showed that the glint over a wavy ocean would have a weak effect on planet overall brightness, itself subject to variation due to clouds and surface changes (ocean/land).

6. Conclusion

In this study, we investigated the potential surface biosignatures that could be detected by Vis-NIR remote sensing on various planetary surface materials, namely, silica sand, liquid water, and water ice particles if they contain pigmented micro-organisms.

We found that, among these surfaces, water ice appears to be the most favorable medium to detect pigmented micro-organisms because of the following:

(1) Water ice is bright and featureless from 0.4 to 0.8 μm, allowing the absorption of any pigment present in the ice to be well noticeable in the form of a strong spectral slope.

(2) The visible phase curve of water ice is the most strongly affected by the presence of pigments. We observed that the visible spectral slope of the pigments contained in water ice particles can change by more than a factor of 3 with phase angles because of the phase reddening effect.

(3) As the water sublimes, potential pigmented micro-organisms initially embedded in the ice can be concentrated at the surface in a sublimation lag deposit. Our measurements show that this process can significantly increase the detectability of the spectral red slope due to the pigment even if they are initially present at low titers in the ice.

While these measurements (spectral reflectance, dependence with phase angle) highlight the capacity of icy surfaces in enabling the identification of pigments with remote sensing techniques, they do not permit confirmation of the biogenic nature of the pigments. The analysis of the spectral dependence of circularly polarized light, which may contain a signal due to the homochirality of living organisms, might provide a way to discriminate biogenic from abiotic pigments (Sparks et al., 2009a). However, more work needs to be done to explore the existence of such a signal and its detectability. For example, is it observable from space in the light scattered by the surface of Earth? Furthermore, our observation of strong phase reddening effect due to biogenic pigment highlight the interest of studying this phenomenon in polarized light in future studies.

These results are of interest for the characterization of the surface of icy worlds in our own solar system, such as Europa or Enceladus. These icy worlds may possess conditions favorable to the emergence of life in their subsurfaces, and the possibility of pigmented microbial life forms being exposed on their surfaces via upwelling events cannot be excluded. Our results suggest, for example, that the visible spectral red slopes of pigments contained in

ice particles are maximized at a phase angle roughly equal to the incidence angle. However, at 60° incidence of irradiance, the spectral slope is maximum at the phase angle where the reflectance is minimum. This may create a challenge for the detection of pigments at large incidence angles. This knowledge can be of interest for the planning of observations made by a probe in fly-by or orbiting an icy satellite. Moreover, the fact that pigments are readily noticeable in ice and can be concentrated at the surface via sublimation highlights the interest of having the capability to observe Europa or Enceladus surfaces with instruments that measure the circular spectro-polarimetry with the intent to discriminate abiotic from biotic pigments.

In the more distant future, the results presented in this study could also be of interest for the search for surface biosignatures in light scattered by distant exoplanets or exomoons. As we discussed in section 3, the signature of biogenic pigments, from photosynthetic or non-photosynthetic organisms, will probably be the easiest surface biosignatures to search for on exoplanets. The data presented in this study show best case "observables" (high signal to noise ratio, S/N) for pigmented micro-organisms (at relatively high concentrations) in silica sand, liquid water, and water ice surfaces that might be encountered in the variety of exoplanets that are potentially habitable. These data can serve as references for observers to evaluate which S/N should be reached by future instruments to detect the spectral features of pigmented micro-organisms.

Apart from the favorability of water ice surfaces for the detection of potential biopigments, we have also shown that liquid water present inside living organisms can mask the spectral features of biomolecules in the near infrared (NIR, 0.9-2.4 μm). Only desiccated cells clearly show absorption bands in the near infrared. Near infrared absorptions of microorganisms mixed in liquid water and water ice are also undetectable. Additionally, these

absorptions in the NIR can also be masked by some atmospheric gases over specific wavelength ranges. But the visible range would generally remain accessible, except in the case of high concentration of aerosols (clouds or organic haze).

Acknowledgements

The construction of the SCITEAS and PHIRE-2 facilities was funded by the University of Bern and by the Swiss National Science Foundation, in particular through the R'equip grant # 206021_133827. We are grateful to all the engineers and technicians of the WP department at the University of Bern who participated in the construction and maintenance of the setups. O.P. thanks Sonia Fornasier for helpful discussions. O.P. also thanks the Center for Space and Habitability of the University of Bern and the National Center for Competence in Research "PlanetS" of the Swiss National Science Foundation for funding. We acknowledge the reviewers for their suggestions and comments, which substantially improved this paper.

Data deposition

The phase curves of *Deinococcus radiodurans* mixed with silica sand, liquid water and water ice particles reported in this paper have been deposited on the Data Analysis Center for Exoplanets (DACE) (https://dace.unige.ch/lossy/index) where they can be freely visualized and downloaded.

Author Disclosure Statement

No competing financial interests exist.

Tables

Wavelength (µm)	0.4-1.4	1.15-1.23	1.37-1.6	1.69-1.78	1.91-1.95	2.05	2.1-2.12	2.17	2.26-2.34
Most absorbing molecules in this range	**pigments**	phospholipids, carbohydrates, (DNA), (proteins) H_2O	carbohydrates, phospholipids, DNA, proteins, H_2O	phospholipids, pigments, proteins, (DNA), (carbohydrates)	carbohydrates, DNA, proteins, phospholipids, H_2O	proteins	carbohydrates	proteins	phospholipids, pigments, carbohydrates, (DNA), (proteins)
Contributing group(s)	–C=C–C=C–…	CH_3, CH_2, CH	O-H, CH_3, CH_2, NH	CH_3, CH_2, CH	O-H, C-O	NH, CO, -C(O)-NH-	O-H	NH, CO, -C(O)-NH-	CH_3, CH_2, CH, OH
Assignment	e^- transitions in molecular orbitals	CH 2nd overtone	OH comb. + 1st overt., NH 1st overt., CH comb. + 1st overt.	CH 1st overtone	OH+CO combination, C=O 2nd overtone	NH+CO+peptide group combinations	OH combination	NH+CO+peptide group combinations	CH-CH and CH-OH combinations

Table 1: Assignment of the visible and near infrared absorption ranges where biomolecules absorb light, as seen in Fig. 2a (Workman Jr and Weyer, 2012).

Surface medium:	*Phase angles at which…*	0° incidence	60° incidence
Silica sand	*...**reflectance** is maximum:*	0°	140°
	*...**red slope** is maximum:*	10-40°	60°
Water ice	*...**reflectance** is maximum:*	0°	140°
	*...**red slope** is maximum:*	0°	60°
Liquid water	*...**reflectance** is maximum:*	0° (specular)	60° (specular)
	*...**red slope** is maximum:*	all (except specular?)	all (except specular?)

Table 2: Phase angles of maximum intensity of reflectance and spectral slope. Phase angles at which the reflectance and the pigment red slope are maximized, for surfaces composed of sand, water ice particles or liquid water illuminated at 0° or 60° incidence.

Figures

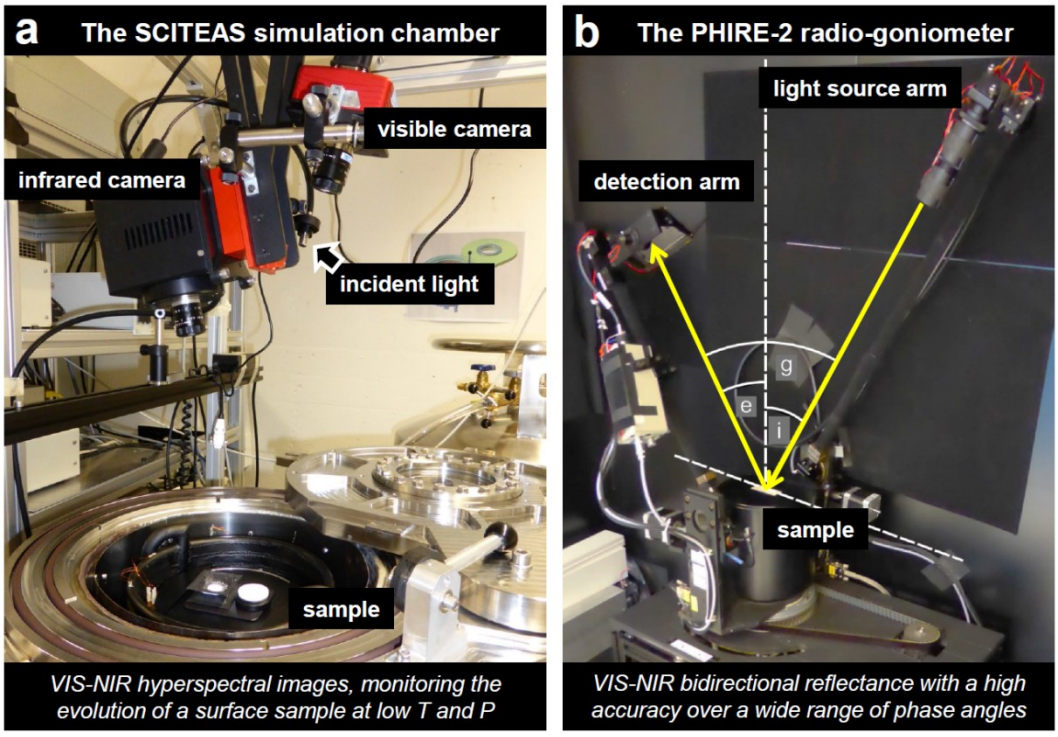

FIG.1. Pictures of the hyperspectral imaging system and the goniometer used to perform the measurements. (a) The SCITEAS simulation chamber (Pommerol et al., 2015). **(b)** The PHIRE-2 radio-goniometer inside the freezer. The incidence angle *i*, emission angle *e*, and phase angle *g* define the observation geometry (Pommerol et al., 2011).

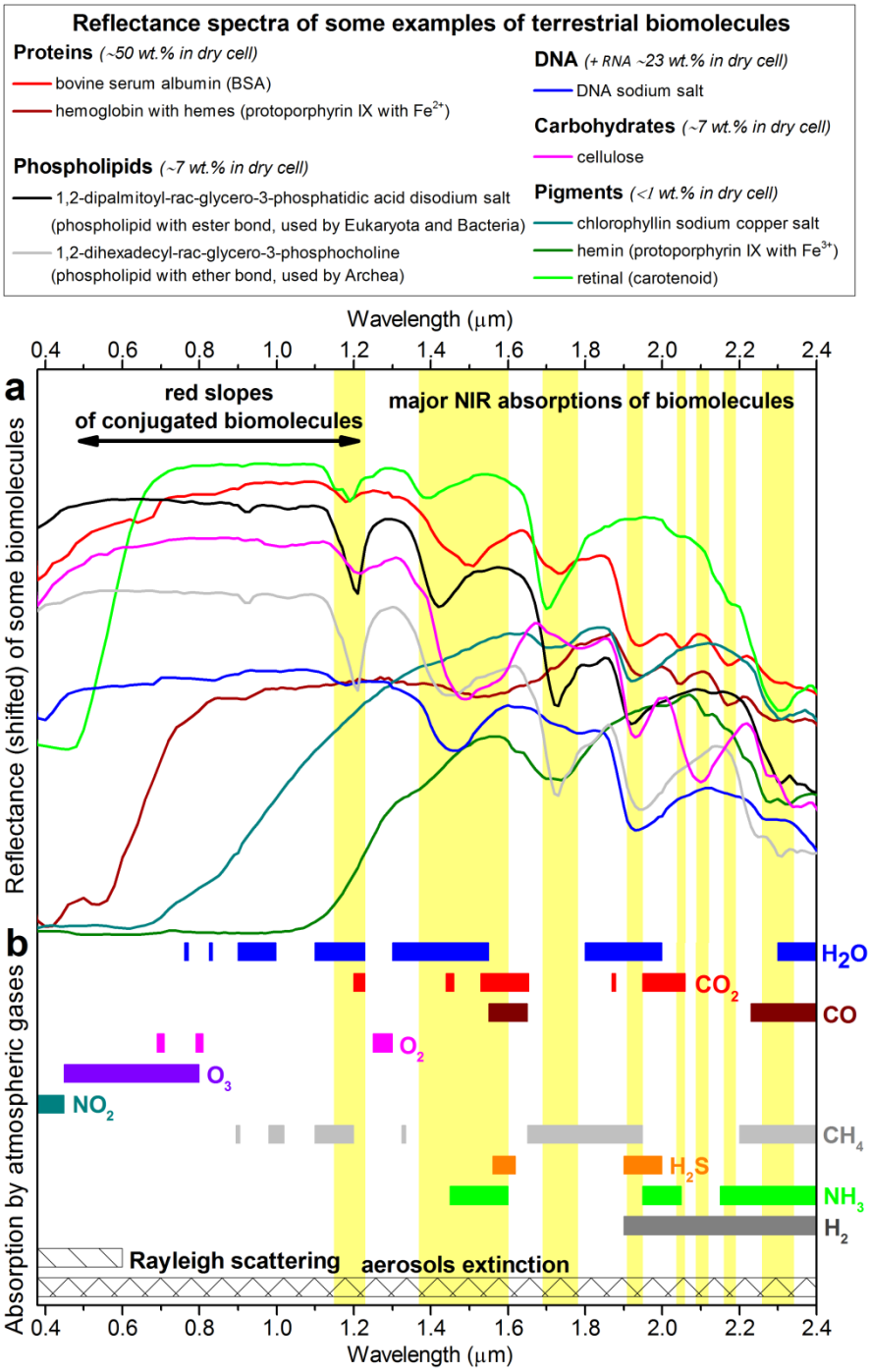

FIG.2. Spectral features of biomolecules versus atmospheric extinctions. (a) Reflectance spectra of some of the main terrestrial biomolecules. Surface biosignatures may be characterized by steep spectral "red" slopes from 0.4 to 1.2 µm due to the absorption by pigments and/or by absorptions bands in the near infrared whose wavelength ranges are indicated in yellow. The detailed assignment of each spectral range is shown in Table 1. **(b)**

Spectral ranges of maximum absorption by potential atmospheric gases on a habitable planet (cross section $>10^{-24}$ cm^2/molecule, obtained from the works of Burrows (2014) and Rothman et al. (2009)). Spectral ranges where Rayleigh scattering or aerosol extinction may occur are also indicated at the very bottom. Depending on the composition of the atmosphere, only some surface biosignatures are potentially detectable through "atmospheric spectral windows."

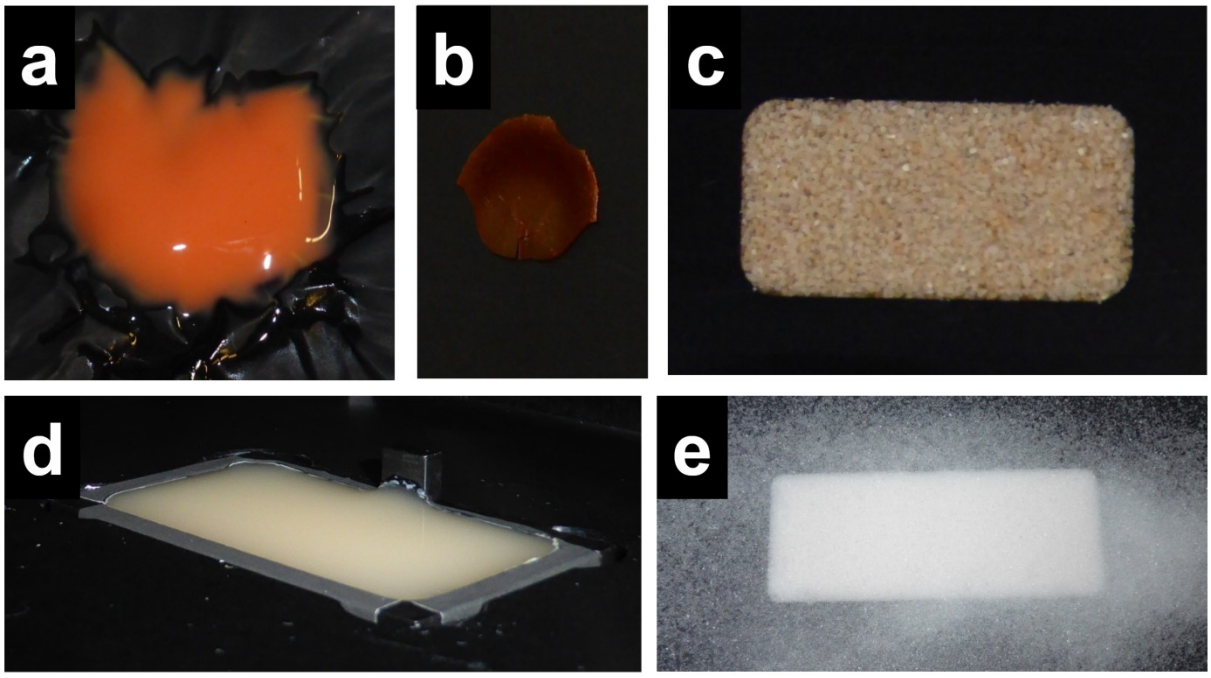

FIG.3. Pictures of the different samples of *Deinococcus radiodurans* measured for this study. (a) Pure hydrated *D. radiodurans*. **(b)** Pure desiccated crust of *D. radiodurans*. **(c)** Silica sand mixed with *D. radiodurans* (10^{10} org./g ≈ 10^{10} org./mL). **(d)** Liquid suspension of *D. radiodurans* (10^{10} org./mL). **(e)** Water ice particles containing inclusions of *D. radiodurans* (10^{10} org./g ≈ 10^{9} org./mL).

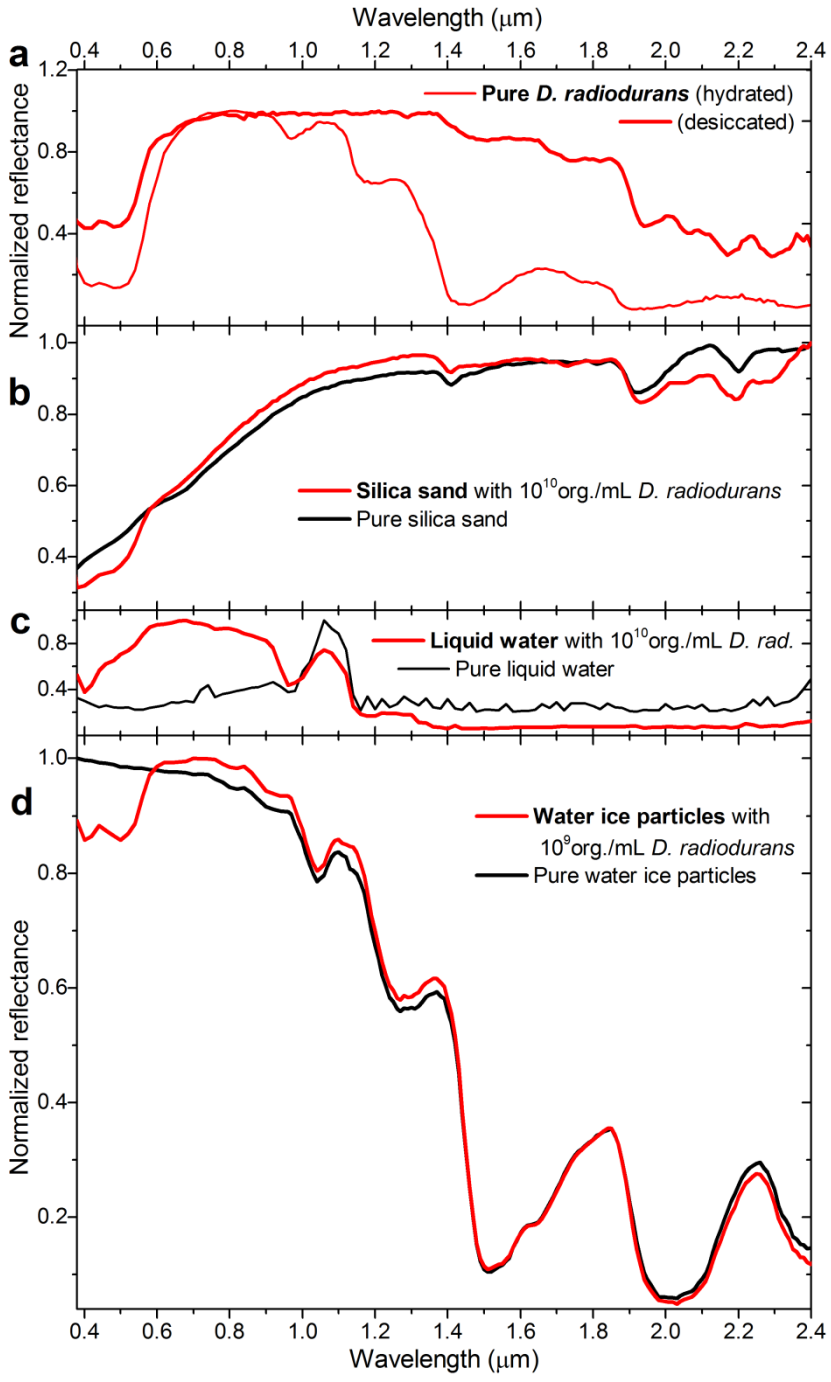

FIG.4. Reflectance spectra of *Deinococcus radiodurans* in various surface media. (a) pure *Deinococcus radiodurans* hydrated and desiccated, **(b)** *D. radiodurans* mixed with silica sand particles (329 μm mean diameter) at a concentration of 10^{10} org./mL (~10^{10} org./g) and pure sand as a reference, **(c)** *D. radiodurans* suspended in liquid water at a concentration of 10^{10} org./mL and pure liquid water as reference, **(d)** *D. radiodurans* in water ice particles at a

concentration of 10^9 org./mL (~10^{10} org./g) and pure water ice particles, measured in the SCITEAS vacuum chamber at about -70°C. N.B.: The reflectance values are normalized by the maximum reflectance in each spectrum. The reader is referred to Fig. 7, 8, and 9 for absolute reflectance values measured with the PHIRE-2 goniometer.

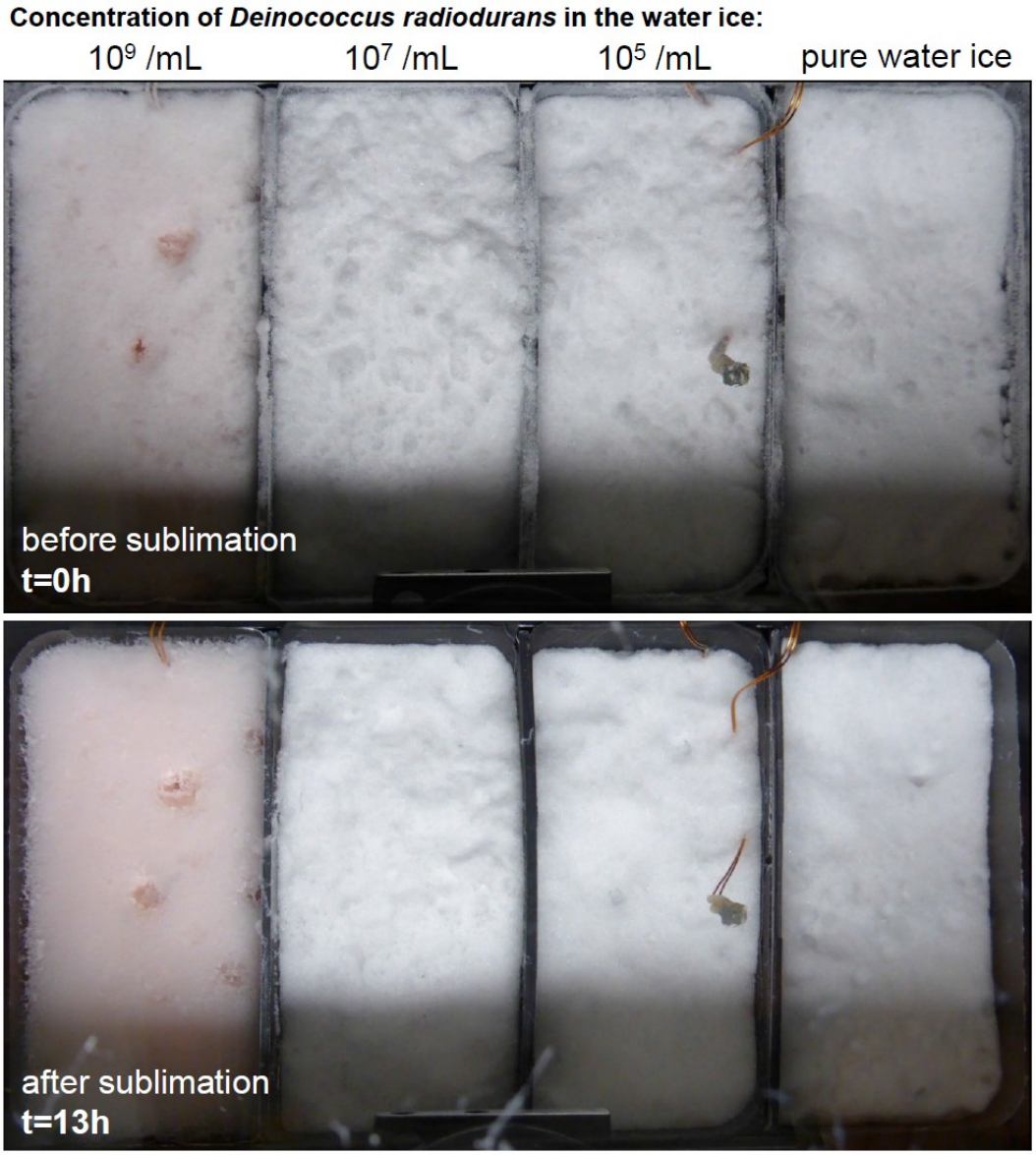

FIG. 5. Picture of the samples of water ice particles inside the SCITEAS simulation chamber before and after 13 hours of sublimation at around 10^{-6} mbar and -70°C. After

sublimation of the first ~5 mm of the ice, a dry deposit of the pigmented bacteria initially present inside the ice particles is formed over the surface of the samples. This deposit has a filamentous texture and is best seen on this image over the most concentrated sample (10^9 org./mL) but is also present over the samples at 10^7 org./mL and 10^5 org./mL in the form of discrete filaments.

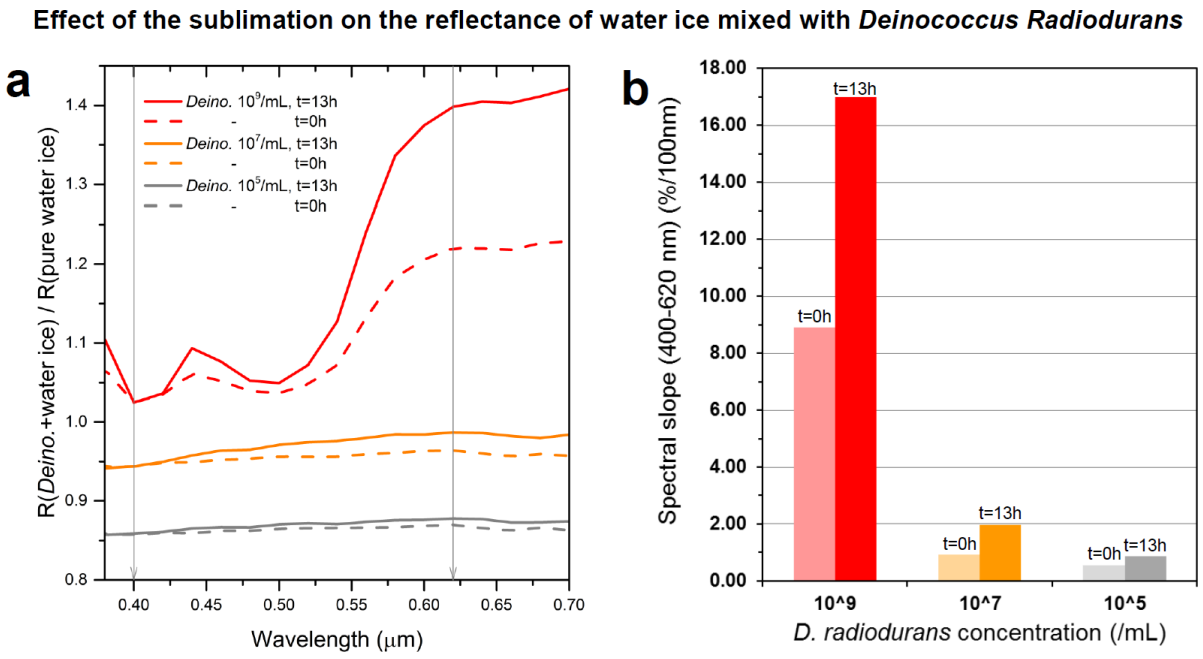

FIG.6. (a) Ratio of the reflectance of the samples of water ice containing *Deinococccus radiodurans* over the reflectance of pure water ice before and after 13 hours of sublimation at 10^{-6} mbar and -70°C. Each curve has been vertically translated for better viewing. **(b)** Evolution of the spectral slope measured from 0.40 to 0.62 µm ($S_r = \frac{R_{0.62}-R_{0.40}}{R_{0.40}\times(620-400)} \times 10^4$) at the surface of the samples before (t = 0 h) and after (t = 13 h) sublimation. At a concentration of 10^7 org./mL and lower, the red slope of the pigments of *Deinococcus radiodurans* is extremely weak. After sublimation of ~5 mm of ice, the slope increases by 50 to 100%.

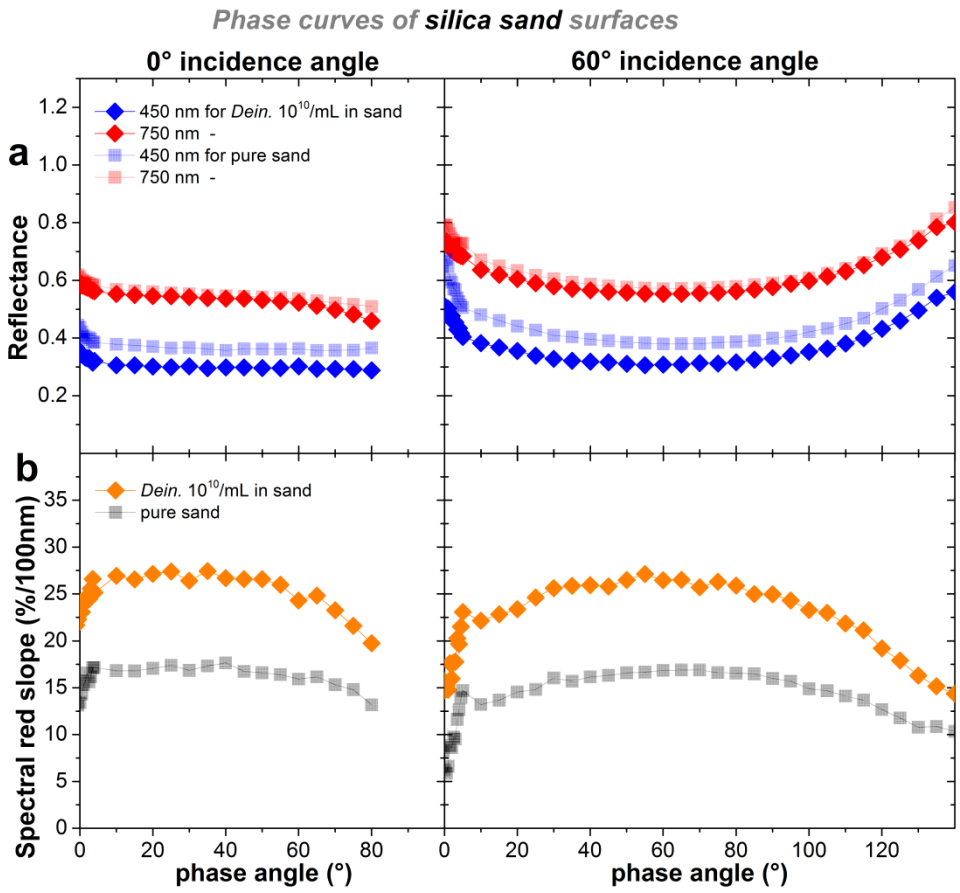

FIG.7. Phase curves and spectral slope of *Deinococcus radiodurans* in silica sand. (a) Phase curves at 0.45 and 0.75 µm and at incidence angles 0° and 60° measured with the PHIRE-2 goniometer for pure sand and sand mixed with 10^{10} org./mL *Deinococcus radiodurans*. **(b)** Relative spectral slope (0.45-0.75 µm) profiles computed from the phase curves using Equation 1. When pigmented bacteria are present in the sand, the spectral slope increases, but its profile over phase angles is similar to pure sand. The data are available on DACE (https://dace.unige.ch/lossy/index).

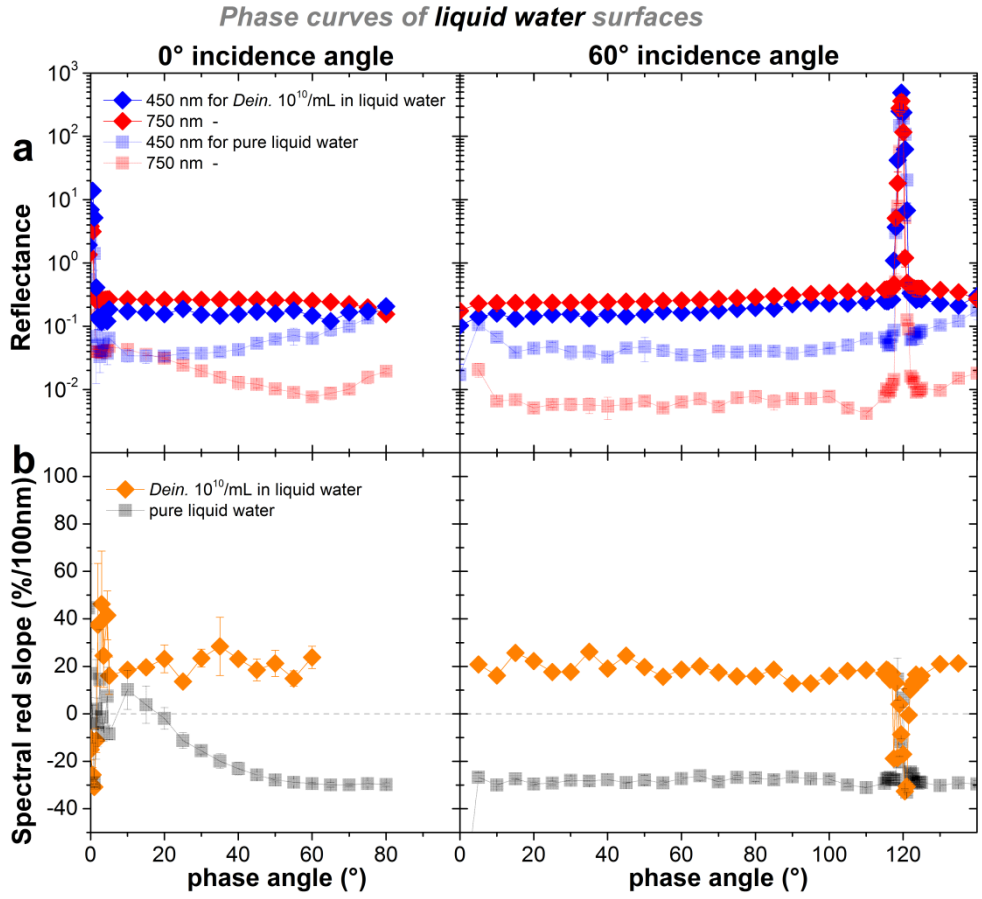

FIG.8. Phase curves and spectral slope of *Deinococcus radiodurans* in liquid water. (a) Phase curves at 0.45 and 0.75 µm and at incidence angles 0° and 60° measured with the PHIRE-2 goniometer for pure liquid water and for a suspension of 10^{10} org./mL *Deinococcus radiodurans* in liquid water. The glint over the liquid surface is materialized by a specular reflection peak at 0° and 120° phase angle respectively. **(b)** Relative spectral slope (0.45-0.75 µm) profiles computed from the phase curves using Equation 1. The slope is redder than that of pure water at all phase angles, except at the specular position where the signal is affected by instrumental artifacts that prevent us to draw any definitive conclusion on the spectral slope at this peculiar geometry. The data are available on DACE (https://dace.unige.ch/lossy/index).

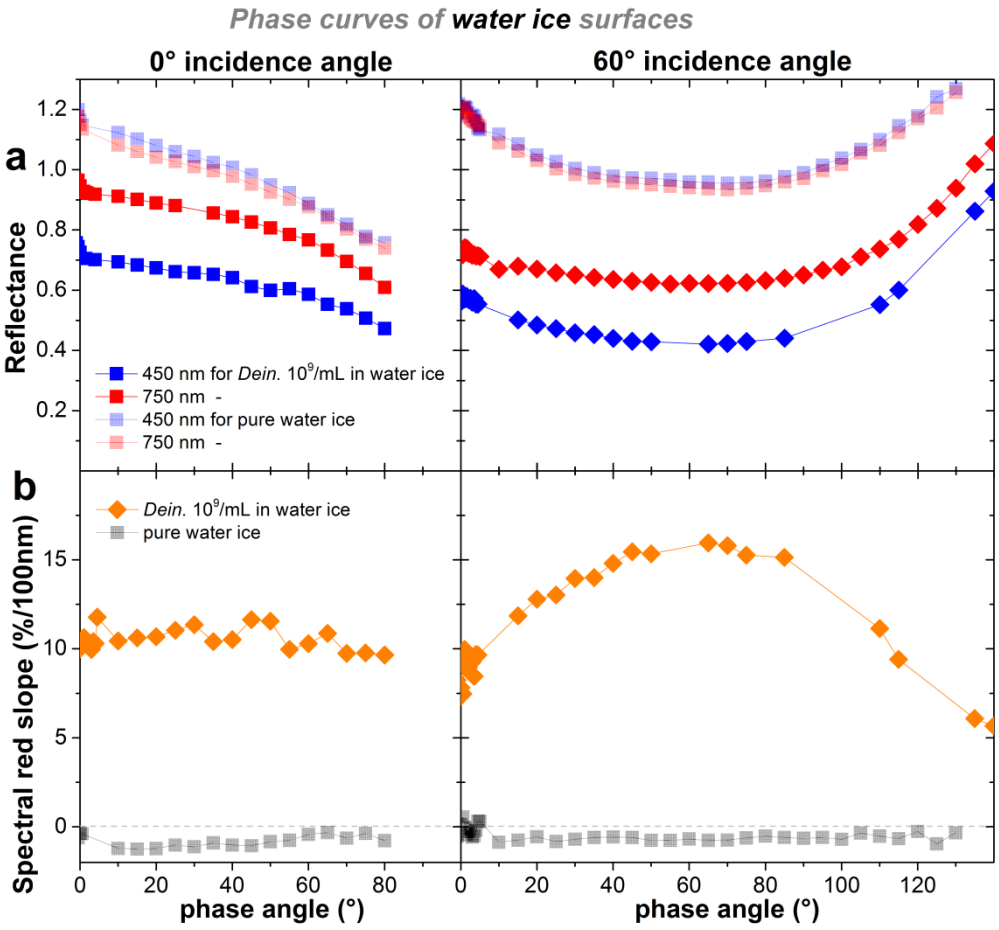

FIG.9. Phase curves and spectral slope of *Deinococcus radiodurans* in water ice grains. **(a)** Phase curves at 0.45 and 0.75 µm and at incidence angles 0° and 60° measured with the PHIRE-2 goniometer for pure water ice grains and water ice grains mixed with 10^9 org./mL *Deinococcus radiodurans*. **(b)** Relative spectral slope (0.45-0.75 µm) profiles computed from the phase curves using Equation 1. At 60° incidence, the relative spectral slope of ice mixed with pigmented bacteria has an arc-shaped profile, due to phase reddening effect (Schröder et al., 2014). The acquisition of the data at 450 nm was erroneous at some phase angles. For clarity, these data are not shown on this figure. The data are available on DACE (https://dace.unige.ch/lossy/index).

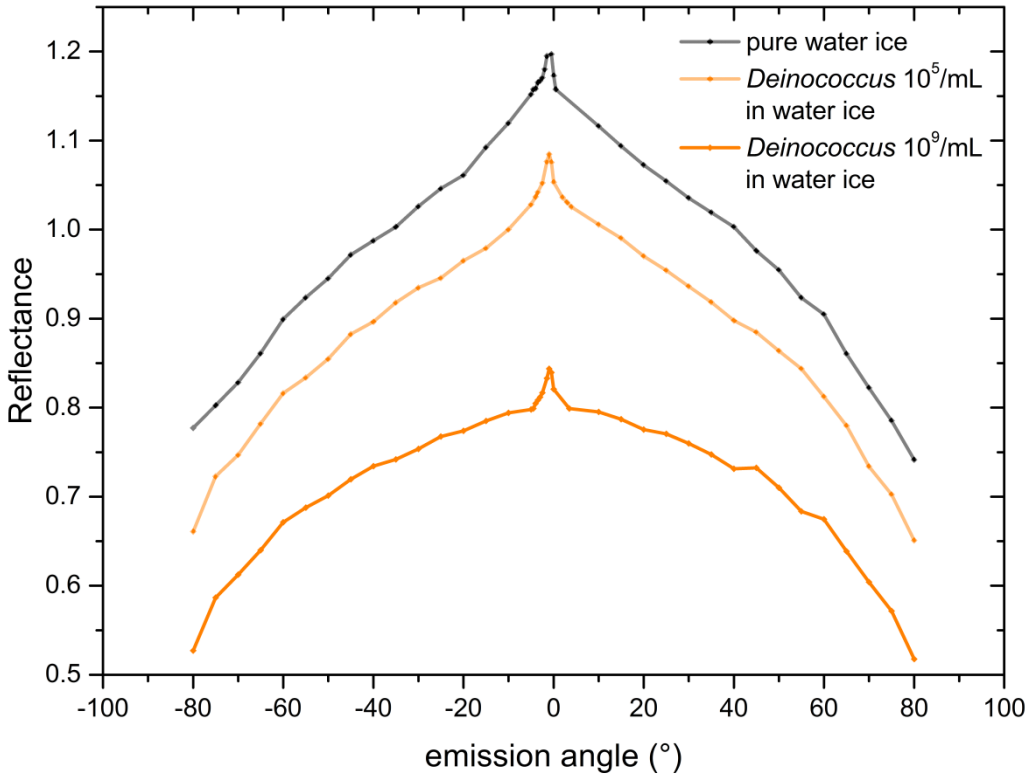

FIG.10. Comparison of the shape of the phase curves measured at 0.55 µm and 0° incidence angle for pure water ice particles and water ice particles containing *Deinococcus radiodurans* at 10^5 org./mL and 10^9 org./mL. As the concentration of *D. radiodurans* increases, the shape of the lateral branches of the phase curve gets more curved, and a discontinuity appears between the basis of the opposition peak and the rest of the phase curve.

References:

Alberts B., Bray D., Hopkin K., Johnson A., Lewis J., Raff M., Roberts K., and Walter P. (2013) Essential cell biology. Garland Science.

Angerhausen D., Sapers H., Citron R., Bergantini A., Lutz S., Queiroz L.L., Alexandre M.d.R., and Araujo A.C.V. (2013) HABEBEE: Habitability of Eyeball-Exo-Earths. *Astrobiology* 13:309-314.

Arnold L. (2008) Earthshine Observation of Vegetation and Implication for Life Detection on Other Planets. In *Strategies of Life Detection*. edited by O. Botta, J. Bada, J. Gomez-Elvira, E. Javaux, F. Selsis and R. Summonss, Springer US, pp 323-333.

Arnold L., Gillet S., Lardiere O., Riaud P., and Schneider J. (2002) A test for the search for life on extrasolar planets: Looking for the terrestrial vegetation signature in the Earthshine spectrum. *Astronomy and Astrophysics* 392:231-237.

Babu P., Kumar R., and Linga P. (2014) Unusual behavior of propane as a co-guest during hydrate formation in silica sand: Potential application to seawater desalination and carbon dioxide capture. *Chemical Engineering Science* 117:342-351.

Bartik K., Bruylants G., Locci E., and Reisse J. (2011) Liquid water: a necessary condition for all life forms? In *Origins and Evolution of Life: An Astrobiological Perspective*. edited by M. Gargaud, P. Lopez-Garcia and H. Martins, Cambridge University Press.

Berdyugina S.V., Kuhn J.R., Harrington D.M., Šantl-Temkiv T., and Messersmith E.J. (2015) Remote sensing of life: polarimetric signatures of photosynthetic pigments as sensitive biomarkers. *International Journal of Astrobiology* FirstView:1-12.

Borucki W.J., Koch D.G., Batalha N., Bryson S.T., Rowe J., Fressin F., Torres G., Caldwell D.A., Christensen-Dalsgaard J., and Cochran W.D. (2012) Kepler-22b: a 2.4 Earth-

radius planet in the habitable zone of a Sun-like star. *The Astrophysical Journal* 745:120.

Burrows A.S. (2014) Spectra as windows into exoplanet atmospheres. *Proceedings of the National Academy of Sciences* 111:12601-12609.

Byrne S. (2009) The Polar Deposits of Mars. *Annual Review of Earth and Planetary Sciences* 37:535-560.

Byrne S., Dundas C.M., Kennedy M.R., Mellon M.T., McEwen A.S., Cull S.C., Daubar I.J., Shean D.E., Seelos K.D., Murchie S.L. and others. (2009) Distribution of Mid-Latitude Ground Ice on Mars from New Impact Craters. *Science* 325:1674-1676.

Campbell A.J., Waddington E.D., and Warren S.G. (2011) Refugium for surface life on Snowball Earth in a nearly-enclosed sea? A first simple model for sea-glacier invasion. *Geophysical Research Letters* 38:L19502.

Chen M., and Blankenship R.E. (2011) Expanding the solar spectrum used by photosynthesis. *Trends Plant Sci* 16:427-431.

Clark R.N. (1999) Spectroscopy of Rocks and Minerals, and Principles of Spectroscopy. In *Manual of Remote Sensing, Volume 3, Remote Sensing for the Earth Sciences*. edited by A.N. Renczs, John Wiley and Sons, New York, pp 3-58.

Clark R.N., Swayze G.A., Wise R., Livo K.E., Hoefen T.M., Kokaly R.F., Sutley S.J., and Team M. (2007) USGS Digital Spectral Library splib05a. edited by D.D.S. 231s, U.S. Geological Survey.

Cleaves H.J., Chalmers J.H., Lazcano A., Miller S.L., and Bada J.L. (2008) A reassessment of prebiotic organic synthesis in neutral planetary atmospheres. *Origins of Life and Evolution of Biospheres* 38:105-115.

Cockell C., Bush T., Bryce C., Direito S., Fox-Powell M., Harrison J., Lammer H., Landenmark H., Martin-Torres J., and Nicholson N. (2016) Habitability: A Review. *Astrobiology* 16:89-117.

Cockell C.S. (2014) Habitable worlds with no signs of life. *Philosophical Transactions of the Royal Society of London A: Mathematical, Physical and Engineering Sciences* 372:20130082.

Cowan N.B., and Strait T.E. (2013) Determining reflectance spectra of surfaces and clouds on exoplanets. *The Astrophysical Journal Letters* 765:L17.

Crow C.A., McFadden L.A., Robinson T., Meadows V.S., Livengood T.A., Hewagama T., Barry R.K., Deming L.D., Lisse C.M., and Wellnitz D. (2011) Views from EPOXI: Colors in Our Solar System as an Analog for Extrasolar Planets. *The Astrophysical Journal* 729:130.

Dalcanton J., Seager S., Aigrain S., Battel S., Brandt N., Conroy C., Feinberg L., Gezari S., Guyon O., and Harris W. (2015) From cosmic birth to living earths: the future of UVOIR space astronomy. Washington, DC, Association for Research in Astronomy (http://arxiv.org/abs/1507.04779).

Dalton J., Cruikshank D., Stephan K., McCord T., Coustenis A., Carlson R., and Coradini A. (2010) Chemical composition of icy satellite surfaces. *Space science reviews* 153:113-154.

Dalton J.B., Mogul R., Kagawa H.K., Chan S.L., and Jamieson C.S. (2003) Near-infrared detection of potential evidence for microscopic organisms on Europa. *Astrobiology* 3:505-529.

Domagal-Goldman S.D., Meadows V.S., Claire M.W., and Kasting J.F. (2011) Using biogenic sulfur gases as remotely detectable biosignatures on anoxic planets. *Astrobiology* 11:419-441.

Domagal-Goldman S.D., Segura A., Claire M.W., Robinson T.D., and Meadows V.S. (2014) Abiotic ozone and oxygen in atmospheres similar to prebiotic Earth. *The Astrophysical Journal* 792:90.

Doughty C.E., and Wolf A. (2010) Detecting Tree-like Multicellular Life on Extrasolar Planets. *Astrobiology* 10:869-879.

Evans T.M., Pont F., Sing D.K., Aigrain S., Barstow J.K., Désert J.-M., Gibson N., Heng K., Knutson H.A., and des Etangs A.L. (2013) The deep blue color of HD 189733b: Albedo measurements with Hubble Space Telescope/Space Telescope Imaging Spectrograph at visible wavelengths. *The Astrophysical Journal Letters* 772:L16.

Fujii Y., and Kawahara H. (2012) Mapping Earth analogs from photometric variability: spin-orbit tomography for planets in inclined orbits. *The Astrophysical Journal* 755:101.

Fujii Y., Kawahara H., Suto Y., Taruya A., Fukuda S., Nakajima T., and Turner E.L. (2010) Colors of a second Earth: estimating the fractional areas of ocean, land, and vegetation of Earth-like exoplanets. *The Astrophysical Journal* 715:866.

García Muñoz A. (2015) Towards a comprehensive model of Earth's disk-integrated Stokes vector. *International Journal of Astrobiology* 14:379-390.

Hale G.M., and Querry M.R. (1973) Optical constants of water in the 200-nm to 200-μm wavelength region. *Appl Opt* 12:555-563.

Hand K., Chyba C., Priscu J., Carlson R., and Nealson K. (2009) Astrobiology and the potential for life on Europa. In *Europa.* University of Arizona Press, Tucson, pp 589-629.

Hapke B. (1993) Theory of Reflectance and Emittance Spectroscopy, Cambridge, United Kingdom.

Harman C., Schwieterman E., Schottelkotte J., and Kasting J. (2015) Abiotic O2 Levels on Planets around F, G, K, and M Stars: Possible False Positives for Life? *The Astrophysical Journal* 812:137.

Hecht E. (2002) Optics. Addison-Wesley.

Hegde S., Paulino-Lima I.G., Kent R., Kaltenegger L., and Rothschild L. (2015) Surface biosignatures of exo-Earths: Remote detection of extraterrestrial life. *Proceedings of the National Academy of Sciences* 112:3886-3891.

Hough J., xa, H, Lucas P., xa, W, Bailey J., xa, A, Tamura M. and others. (2006) PlanetPol: A Very High Sensitivity Polarimeter. *Publications of the Astronomical Society of the Pacific* 118:1302-1318.

Howard A.W., Sanchis-Ojeda R., Marcy G.W., Johnson J.A., Winn J.N., Isaacson H., Fischer D.A., Fulton B.J., Sinukoff E., and Fortney J.J. (2013) A rocky composition for an Earth-sized exoplanet. *Nature* 503:381-384.

Hsu H.-W., Postberg F., Sekine Y., Shibuya T., Kempf S., Horányi M., Juhász A., Altobelli N., Suzuki K., and Masaki Y. (2015) Ongoing hydrothermal activities within Enceladus. *Nature* 519:207-210.

1 Kaltenegger L., and Selsis F. (2007) Biomarkers set in context. In *Extrasolar planets:*
2 *formation, detection and dynamics*. edited by R. Dvoraks, John Wiley & Sons, pp 79-
3 98.

4 Kasting J.F., Whitmire D.P., and Reynolds R.T. (1993) Habitable Zones around Main
5 Sequence Stars. *Icarus* 101:108-128.

6 Kawahara H., and Fujii Y. (2010) Global mapping of Earth-like exoplanets from scattered
7 light curves. *The Astrophysical Journal* 720:1333.

8 Kiang N.Y., Siefert J., and Blankenship R.E. (2007) Spectral signatures of photosynthesis. I.
9 Review of earth organisms. *Astrobiology* 7:222-251.

10 Kopparapu R.K. (2013) A Revised Estimate of the Occurrence Rate of Terrestrial Planets in
11 the Habitable Zones around Kepler M-dwarfs. *The Astrophysical Journal Letters*
12 767:L8.

13 Labandeira C.C. (2005) Invasion of the continents: cyanobacterial crusts to tree-inhabiting
14 arthropods. *Trends in Ecology & Evolution* 20:253-262.

15 Lammer H., Bredehöft J., Coustenis A., Khodachenko M., Kaltenegger L., Grasset O., Prieur
16 D., Raulin F., Ehrenfreund P., Yamauchi M. and others. (2009) What makes a planet
17 habitable? *Astronomy and Astrophysics Review* 17:181-249.

18 Léger A., Selsis F., Sotin C., Guillot T., Despois D., Mawet D., Ollivier M., Labèque A.,
19 Valette C., Brachet F. and others. (2004) A new family of planets? "Ocean-Planets".
20 *Icarus* 169:499-504.

21 Lemee L., Peuchant E., Clerc M., Brunner M., and Pfander H. (1997) Deinoxanthin: A new
22 carotenoid isolated from Deinococcus radiodurans. *Tetrahedron* 53:919-926.

Liebig M.A., Franzluebbers A.J., and Follett R.F. (2012) Managing Agricultural Greenhouse Gases: Coordinated Agricultural Research Through GRACEnet to Address Our Changing Climate. Academic Press.

Liu G.Y., and Nizet V. (2009) Color me bad: microbial pigments as virulence factors. *Trends Microbiol* 17:406-413.

Lysenko V., Chistyakov V., Zimakov D., Soier V., Sazykina M., Sazykina M., Sazykin I., and Krasnov V. (2011) Separation and mass spectrometry identification of carotenoid complex from radioresistant bacteria Deinococcus radiodurans. *Journal of Analytical Chemistry* 66:1281-1284.

Makarova K.S., Aravind L., Wolf Y.I., Tatusov R.L., Minton K.W., Koonin E.V., and Daly M.J. (2001) Genome of the Extremely Radiation-Resistant Bacterium Deinococcus radiodurans Viewed from the Perspective of Comparative Genomics. *Microbiol Mol Biol Rev* 65:44-79.

Marchant D., Lewis A.R., Phillips W.M., Moore E., Souchez R., Denton G.H., Sugden D., Potter N., and Landis G.P. (2002) Formation of patterned ground and sublimation till over Miocene glacier ice in Beacon Valley, southern Victoria Land, Antarctica. *Geological Society of America Bulletin* 114:718-730.

Martin W.E., Hesse E., Hough J.H., Sparks W.B., Cockell C.S., Ulanowski Z., Germer T.A., and Kaye P.H. (2010) Polarized optical scattering signatures from biological materials. *Journal of Quantitative Spectroscopy and Radiative Transfer* 111:2444-2459.

Martin W.E., Hesse E., Hough J.H., and Gledhill T.M. (2016) High-sensitivity Stokes spectropolarimetry on cyanobacteria. *Journal of Quantitative Spectroscopy and Radiative Transfer* 170:131-141.

Martins J., Santos N., Figueira P., Faria J., Montalto M., Boisse I., Ehrenreich D., Lovis C., Mayor M., and Melo C. (2015) Evidence for a spectroscopic direct detection of reflected light from 51 Pegasi b. *Astronomy & Astrophysics* 576:A134.

Meadows V.S., and Seager S. (2010) Terrestrial Planet Atmospheres and Biosignatures. In *Exoplanets*. edited by S. Seager, R.Ž. Dotson and L.P. Institutes, University of Arizona Press, pp 441-470.

Milgrom L.R. (1997) The colours of life: an introduction to the chemistry of porphyrins and related compounds. Oxford University Press.

Miller R.L., Castillo C.E.D., and McKee B.A. (2007) Remote Sensing of Coastal Aquatic Environments: Technologies, Techniques and Applications. Springer Netherlands.

Montañés-Rodríguez P., Pallé E., Goode P., and Martín-Torres F. (2006) Vegetation signature in the observed globally integrated spectrum of Earth considering simultaneous cloud data: applications for extrasolar planets. *The Astrophysical Journal* 651:544.

Moore J.M., Black G., Buratti B., Phillips C.B., Spencer J., and Sullivan R. (2009) Surface properties, regolith, and landscape degradation. In *Europa.* University of Arizona Press, Tucson, pp 329-349.

Pascal R. (2016) Physicochemical Requirements Inferred for Chemical Self-Organization Hardly Support an Emergence of Life in the Deep Oceans of Icy Moons. *Astrobiology* 16:328-334.

Pepe F., Cameron A.C., Latham D.W., Molinari E., Udry S., Bonomo A.S., Buchhave L.A., Charbonneau D., Cosentino R., Dressing C.D. and others. (2013) An Earth-sized planet with an Earth-like density. *Nature* 503:377-380.

Pierrehumbert R.T. (2011) A Palette of Climates for Gliese 581g. *The Astrophysical Journal Letters* 726:L8.

Pierrehumbert R.T., Abbot D.S., Voigt A., and Koll D. (2011) Climate of the Neoproterozoic. *Annual Review of Earth and Planetary Sciences* 39:417-460.

Poch O., Pommerol A., Jost B., Carrasco N., Szopa C., and Thomas N. (2016a) Sublimation of ice–tholins mixtures: A morphological and spectro-photometric study. *Icarus* 266:288-305.

Poch O., Pommerol A., Jost B., Carrasco N., Szopa C., and Thomas N. (2016b) Sublimation of water ice mixed with silicates and tholins: Evolution of surface texture and reflectance spectra, with implications for comets. *Icarus* 267:154-173.

Pommerol A., Jost B., Poch O., El-Maarry M.R., Vuitel B., and Thomas N. (2015) The SCITEAS experiment: Optical characterizations of Sublimating icy planetary analogues. *Planetary and Space Science* 109:106-122.

Pommerol A., Thomas N., Affolter M., Portyankina G., Jost B., Seiferlin K., and Aye K.M. (2011) Photometry and bulk physical properties of Solar System surfaces icy analogs: The Planetary Ice Laboratory at University of Bern. *Planetary and Space Science* 59:1601-1612.

Porco C., Helfenstein P., Thomas P., Ingersoll A., Wisdom J., West R., Neukum G., Denk T., Wagner R., and Roatsch T. (2006) Cassini observes the active south pole of Enceladus. *Science* 311:1393-1401.

Quintana E.V., Barclay T., Raymond S.N., Rowe J.F., Bolmont E., Caldwell D.A., Howell S.B., Kane S.R., Huber D., and Crepp J.R. (2014) An Earth-sized planet in the habitable zone of a cool star. *Science* 344:277-280.

Reba M.L., Pomeroy J., Marks D., and Link T.E. (2012) Estimating surface sublimation losses from snowpacks in a mountain catchment using eddy covariance and turbulent transfer calculations. *Hydrological Processes* 26:3699-3711.

Robinson T.D., Ennico K., Meadows V.S., Sparks W., Bussey D.B.J., Schwieterman E.W., and Breiner J. (2014) Detection of ocean glint and ozone absorption using LCROSS Earth observations. *The Astrophysical Journal* 787:171.

Robinson T.D., Meadows V.S., and Crisp D. (2010) Detecting oceans on extrasolar planets using the glint effect. *The Astrophysical Journal Letters* 721:L67.

Robinson T.D., Stapelfeldt K.R., and Marley M.S. (2016) Characterizing Rocky and Gaseous Exoplanets with 2 m Class Space-based Coronagraphs. *Publications of the Astronomical Society of the Pacific* 128:025003.

Roth L., Saur J., Retherford K.D., Strobel D.F., Feldman P.D., McGrath M.A., and Nimmo F. (2014) Transient Water Vapor at Europa's South Pole. *Science* 343:171-174.

Rothman L.S., Gordon I.E., Barbe A., Benner D.C., Bernath P.F., Birk M., Boudon V., Brown L.R., Campargue A., Champion J.P. and others. (2009) The HITRAN 2008 molecular spectroscopic database. *Journal of Quantitative Spectroscopy and Radiative Transfer* 110:533-572.

Sagan C., Thompson W.R., Carlson R., Gurnett D., and Hord C. (1993) A search for life on Earth from the Galileo spacecraft. *Nature* 365:715-721.

Sanromá E., Pallé E., and Munõz A.G. (2013) On the effects of the evolution of microbial mats and land plants on the Earth as a planet. Photometric and spectroscopic light curves of paleo-Earths. *The Astrophysical Journal* 766:133.

Sanromá E., Pallé E., Parenteau M.N., Kiang N.Y., Gutiérrez-Navarro A.M., López R., and Montañés-Rodríguez P. (2014) Characterizing the Purple Earth: Modeling the Globally Integrated Spectral Variability of the Archean Earth. *The Astrophysical Journal* 780:52.

Scalo J., Kaltenegger L., Segura A., Fridlund M., Ribas I., Kulikov Y.N., Grenfell J.L., Rauer H., Odert P., and Leitzinger M. (2007) M stars as targets for terrestrial exoplanet searches and biosignature detection. *Astrobiology* 7:85-166.

Schröder S.E., Grynko Y., Pommerol A., Keller H.U., Thomas N., and Roush T.L. (2014) Laboratory observations and simulations of phase reddening. *Icarus* 239:201-216.

Schwieterman E.W., Cockell C.S., and Meadows V.S. (2015) Nonphotosynthetic Pigments as Potential Biosignatures. *Astrobiology* 15:341-361.

Seager S. (2014) The future of spectroscopic life detection on exoplanets. *Proceedings of the National Academy of Sciences* 111:12634-12640.

Seager S., Turner E.L., Schafer J., and Ford E.B. (2005) Vegetation's red edge: a possible spectroscopic biosignature of extraterrestrial plants. *Astrobiology* 5:372-390.

Segura A., Kasting J.F., Meadows V., Cohen M., Scalo J., Crisp D., Butler R.A., and Tinetti G. (2005) Biosignatures from Earth-like planets around M dwarfs. *Astrobiology* 5:706-725.

Segura A., Walkowicz L.M., Meadows V., Kasting J., and Hawley S. (2010) The effect of a strong stellar flare on the atmospheric chemistry of an Earth-like planet orbiting an M dwarf. *Astrobiology* 10:751-771.

Shporer A., and Hu R. (2015) Studying atmosphere-dominated hot Jupiter Kepler phase curves: Evidence that inhomogeneous atmospheric reflection is common. *The Astronomical Journal* 150:112.

Sparks W., Germer T.A., MacKenty J.W., and Snik F. (2012) Compact and robust method for full Stokes spectropolarimetry. *Appl Opt* 51:5495-5511.

Sparks W.B., Hough J., Germer T.A., Chen F., DasSarma S., DasSarma P., Robb F.T., Manset N., Kolokolova L., and Reid N. (2009a) Detection of circular polarization in light scattered from photosynthetic microbes. *Proceedings of the National Academy of Sciences* 106:7816-7821.

Sparks W.B., Hough J.H., Kolokolova L., Germer T.A., Chen F., DasSarma S., DasSarma P., Robb F.T., Manset N., Reid I.N. and others. (2009b) Circular polarization in scattered light as a possible biomarker. *Journal of Quantitative Spectroscopy and Radiative Transfer* 110:1771-1779.

Sterzik M.F., Bagnulo S., and Palle E. (2012) Biosignatures as revealed by spectropolarimetry of Earthshine. *Nature* 483:64-66.

Takeuchi N., Dial R., Kohshima S., Segawa T., and Uetake J. (2006) Spatial distribution and abundance of red snow algae on the Harding Icefield, Alaska derived from a satellite image. *Geophysical research letters* 33:L21502.

Tarter J.C., Backus P.R., Mancinelli R.L., Aurnou J.M., Backman D.E., Basri G.S., Boss A.P., Clarke A., Deming D., and Doyle L.R. (2007) A reappraisal of the habitability of planets around M dwarf stars. *Astrobiology* 7:30-65.

Tian F., France K., Linsky J.L., Mauas P.J.D., and Vieytes M.C. (2014) High stellar FUV/NUV ratio and oxygen contents in the atmospheres of potentially habitable planets. *Earth and Planetary Science Letters* 385:22-27.

Tinetti G., Meadows V.S., Crisp D., Kiang N.Y., Kahn B.H., Bosc E., Fishbein E., Velusamy T., and Turnbull M. (2006) Detectability of planetary characteristics in disk-averaged spectra II: synthetic spectra and light-curves of Earth. *Astrobiology* 6:881-900.

Ting C.S., Rocap G., King J., and Chisholm S.W. (2002) Cyanobacterial photosynthesis in the oceans: the origins and significance of divergent light-harvesting strategies. *Trends Microbiol* 10:134-142.

Torsvik V., Goksøyr J., and Daae F.L. (1990) High diversity in DNA of soil bacteria. *Appl Environ Microbiol* 56:782-787.

Westall F., Loizeau D., Foucher F., Bost N., Betrand M., Vago J., and Kminek G. (2013) Habitability on Mars from a microbial point of view. *Astrobiology* 13:887-897.

Williams D.M., and Gaidos E. (2008) Detecting the glint of starlight on the oceans of distant planets. *Icarus* 195:927-937.

Woolf N.J., Smith P.S., Traub W.A., and Jucks K.W. (2002) The spectrum of Earthshine: a pale blue dot observed from the ground. *The Astrophysical Journal* 574:430.

Wordsworth R., and Pierrehumbert R. (2014) Abiotic Oxygen-dominated Atmospheres on Terrestrial Habitable Zone Planets. *The Astrophysical Journal Letters* 785:L20.

Workman Jr J., and Weyer L. (2012) Practical guide and spectral atlas for interpretive near-infrared spectroscopy. CRC Press.

Zolotov M.Y., and Kargel J. (2009) On the chemical composition of Europa's icy shell, ocean, and underlying rocks. *Europa*, edited by R.T. Pappalardo, W.B. McKinnon, and K. Khurana, University of Arizona Press, Tucson, AZ, 431-458.

Remote sensing of potential biosignatures from rocky, liquid or icy (exo)planetary surfaces

Olivier Poch, Joachim Frey, Isabel Roditi, Antoine Pommerol, Bernhard Jost, and Nicolas Thomas

Supplementary Material

#S1: Descriptions and structures of the biomolecules measured in this work

#S2: Reflectance of whole organisms

#S3: Influence of the viewing geometry on the pigment's spectral slope.

#S1: Descriptions and structures of the biomolecules measured in this work

Name	Provider, reference	Chemical structure
bovine serum albumin (BSA)	Sigma-Aldrich, n°A7638	polypeptide, i.e. polymer of amino acids joined by a covalent bond (peptide bond)
hemoglobin human	Sigma-Aldrich, n°H7379	polypeptide + hemes (protoporphyrin IX with Fe^{2+})
1,2-dipalmitoyl-rac-glycero-3-phosphatidic acid disodium salt	Bachem, n°O-1190.0250	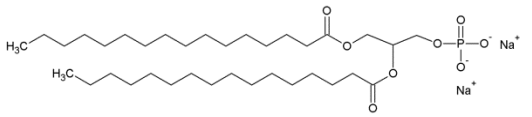
1,2-dihexadecyl-*rac*-glycero-3-phosphocholine	Sigma-Aldrich, n°P3777	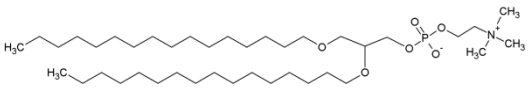
deoxyribonucleic acid sodium salt, from calf thymus (DNA)	Sigma-Aldrich, n°D1501	polymer of nucleotides, each nucleotide is composed of a nucleobase (guanine, adenine, cytosine, and thymine), linked to a backbone made of sugars (deoxyribose) and phosphate groups
cellulose	Sigma-Aldrich, n°310697	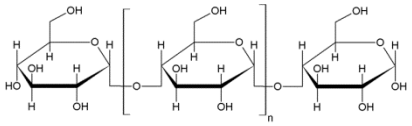
chlorophyllin sodium copper salt	Sigma-Aldrich, n°C6003	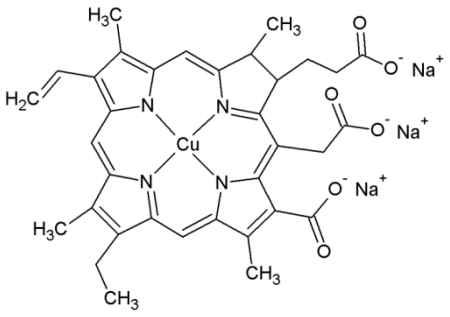

hemin (protoporphyrin IX with Fe^{3+})	Sigma-Aldrich, n°51280	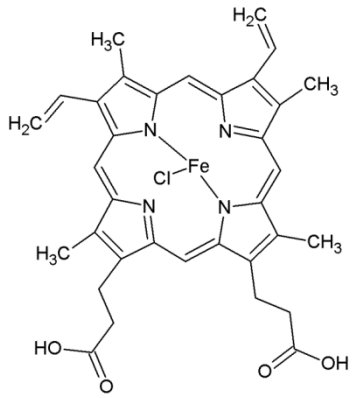
retinal	Sigma-Aldrich, n°R2500	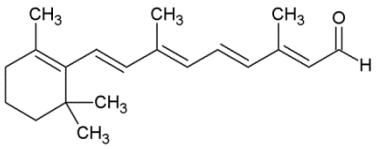

Table S1: List of the biomolecules measured for this study.

#S2: Reflectance of whole organisms

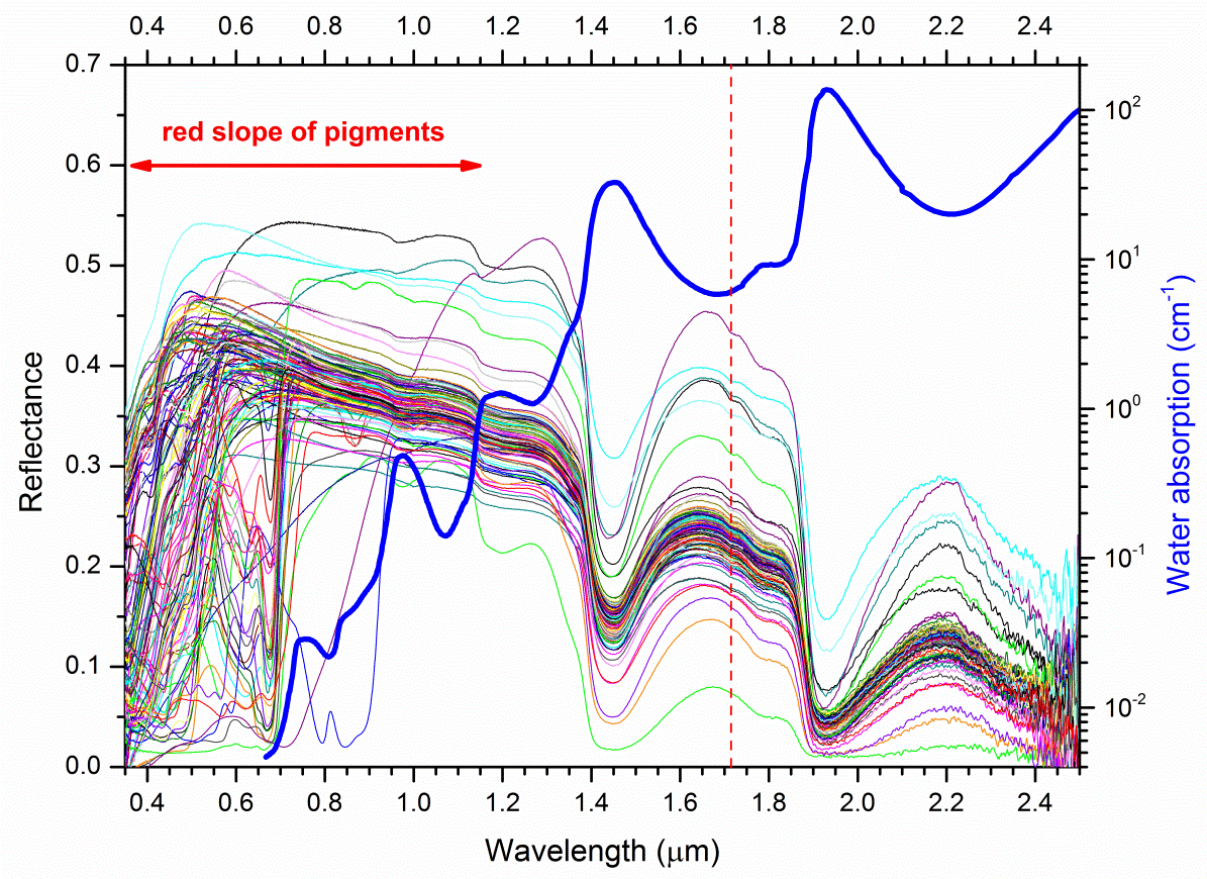

Fig. S1: Reflectance spectra of the 137 living microorganisms measured by (Hegde et al., 2015) and absorption spectrum of liquid water (Kou et al., 1993). The red slopes of pigments occur from about 0.4 to 1.2 μm. Absorption bands due to water of hydration dominate the infrared spectrum of microorganisms, with absorption bands centred at about 1.2, 1.45, 1.78, 1.9 and 2.4 μm. In the near infrared, only one very weak C–H absorption band can be detected at about 1.71 μm, and only for some microorganisms (vertical red dashed line).

#S3: Influence of the viewing geometry on the pigment's spectral slope.

Quantification of the spectral slope

We quantified the slope (or color) in two different ways. First we computed the difference of reflectance to retrieve the "absolute" spectral slope, S (in %/100 nm):

$$S = \frac{R_{0.75} - R_{0.45}}{750 - 450} \times 10^4 \qquad \text{(Equation S1)}$$

with $R_{0.75}$ and $R_{0.45}$ the reflectance (from 0 to 1) measured at 0.75 and 0.45 μm respectively. In practice, this value is determined when the absolute values of reflectance can be measured.

Second, we computed the relative spectral slope, or "relative magnitude of slope", S_r (in %/100 nm):

$$S_r = \frac{R_{0.75} - R_{0.45}}{R_{0.45} \times (750 - 450)} \times 10^4 \qquad \text{(Equation S2)}$$

In practice, this value is determined when only relative values of reflectance can be measured. As the phase angle varies, those two definitions of the slope can behave differently. The phase curves measured at 0° and 60° and the resulting spectral slope profiles are presented in Fig. S2, Fig. S3 and Fig. S4.

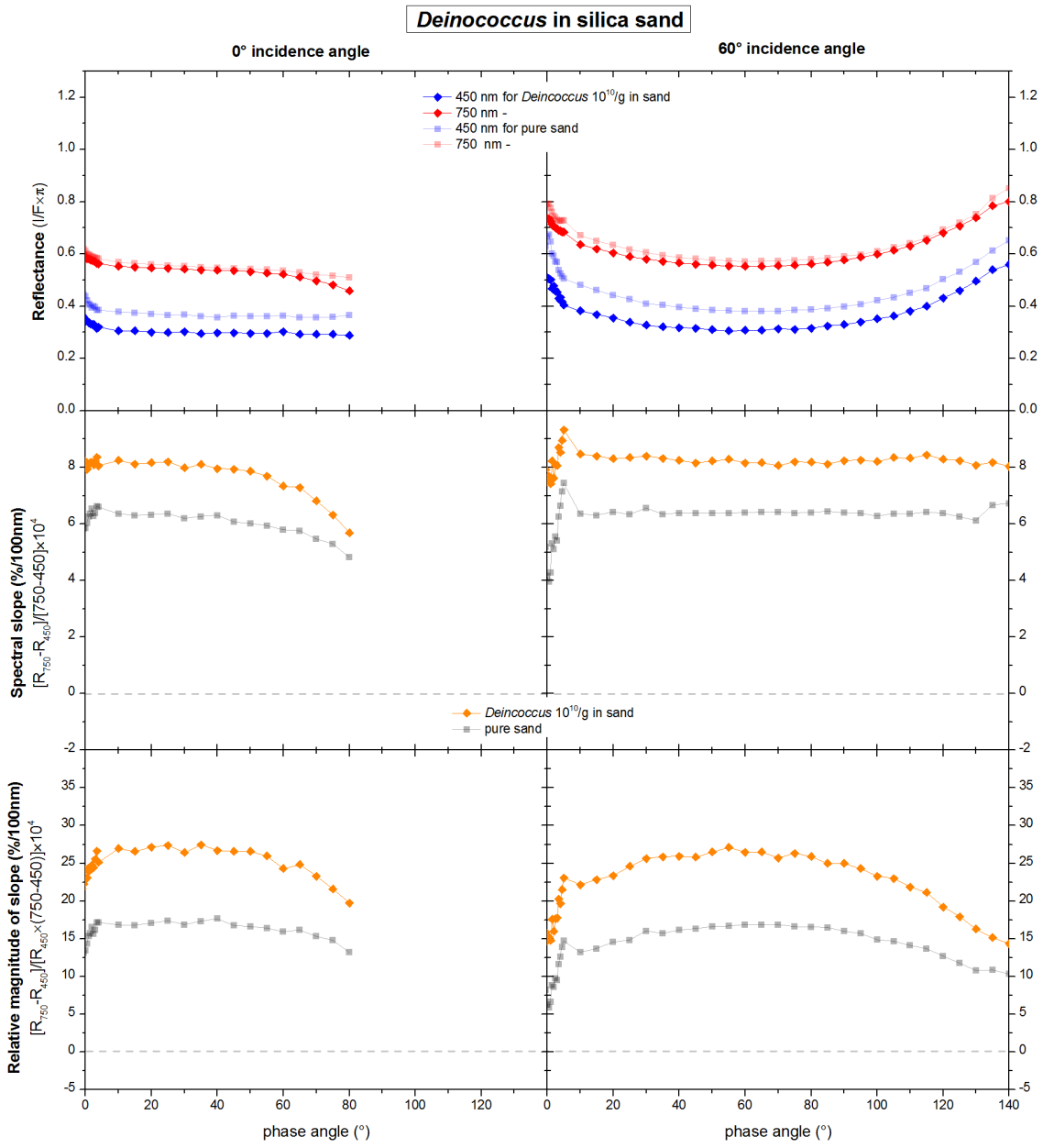

1

2 **Fig. S2: (a)** Phase curves at 0.45 and 0.75 µm and at incidence angles 0° and 60° measured with the
3 PHIRE-2 goniometer for pure sand and sand mixed with 10^{10} org./g (≈ 10^{10} org./mL) *Deinococcus*
4 *radiodurans*. **(b)** Spectral slope (0.45-0.75 µm) profiles computed from the phase curves using
5 Equation S1. **(c)** Relative spectral slope (0.45-0.75 µm) profiles computed from the phase curves using
6 Equation S2.

7

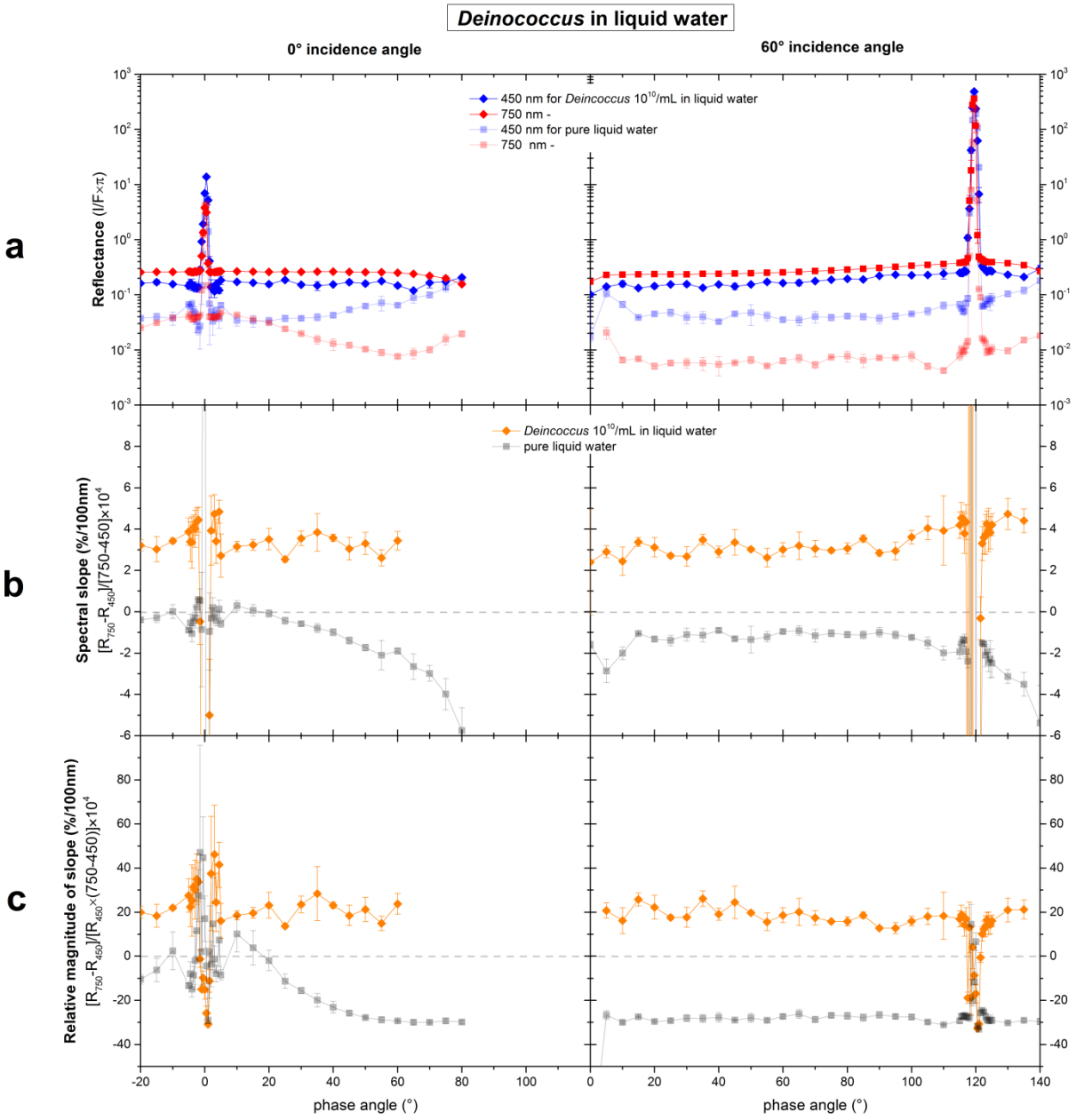

Fig. S3: (a) Phase curves at 0.45 and 0.75 µm and at incidence angles 0° and 60° measured with the PHIRE-2 goniometer for pure liquid water and liquid water mixed with 10^{10} org./mL *Deinococcus radiodurans*. The data points at 0.45 µm are the average of two measurements, done to improve the signal to noise ratio on this relatively dark sample. **(b)** Spectral slope (0.45-0.75 µm) profiles computed from the phase curves using Equation S1. **(c)** Relative spectral slope (0.45-0.75 µm) profiles computed from the phase curves using Equation S2.

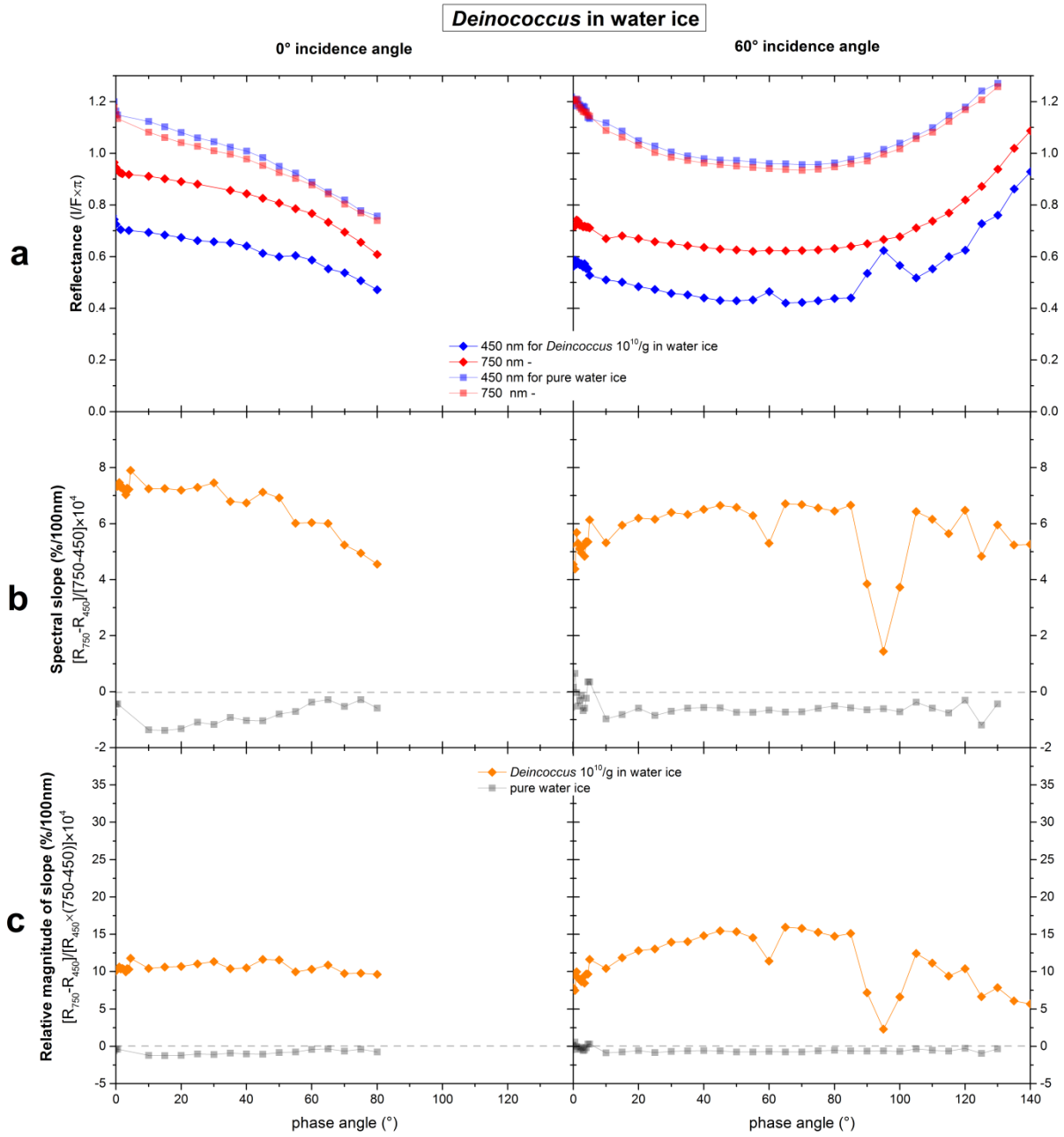

Fig. S4: (a) Phase curves at 0.45 and 0.75 µm and at incidence angles 0° and 60° measured with the PHIRE-2 goniometer for pure water ice particles and water ice particles containing 10^{10} org./g (≈ 10^9 org./mL) *Deinococcus radiodurans*. **(b)** Spectral slope (0.45-0.75 µm) profiles computed from the phase curves using Equation S1. **(c)** Relative spectral slope (0.45-0.75 µm) profiles computed from the phase curves using Equation S2. The acquisition of the data at 450 nm was erroneous at some phase angles. However, these bad points do not prevent the interpretation of the general trend of the phase curves. These data points have been removed for clarity on Fig. 9.

References:

Hegde S, Paulino-Lima IG, Kent R, Kaltenegger L, and Rothschild L. (2015) Surface biosignatures of exo-Earths: Remote detection of extraterrestrial life. *Proceedings of the National Academy of Sciences*, 112, 3886-3891.

Kou L, Labrie D, and Chylek P. (1993) Refractive indices of water and ice in the 0.65-to 2.5-μm spectral range. *Appl Opt*, 32, 3531-3540.